ORNL/TM-2018/842

Oak Ridge National Laboratory SiC/SiC Composites Technology Gap Analysis for Molten Salt Reactors

Josina W. Geringer
Takaaki Koyanagi
Yoonjo Lee
Yutai Katoh

June 2018

OAK RIDGE NATIONAL LABORATORY
MANAGED BY UT-BATTELLE FOR THE US DEPARTMENT OF ENERGY

ORNL/TM-2018/842

Material Science and Technology Division

SIC/SIC COMPOSITES TECHNOLOGY GAP ANALYSIS FOR MOLTEN SALT REACTORS

Authors:

Josina W. Geringer
Takaaki Koyanagi
Yoonjo Lee
Yutai Katoh

Date Published:

June 2018

Prepared by
OAK RIDGE NATIONAL LABORATORY
Oak Ridge, TN 37831-6283
managed by
UT-BATTELLE, LLC
for the
US DEPARTMENT OF ENERGY
under contract DE-AC05-00OR22725

CONTENTS

LIST OF FIGURES

LIST OF TABLES

ABBREVIATIONS, ACRONYMS, AND INITIALISMS

AHTR	Advanced High Temperature Reactor
ARE	Aircraft Reactor Experiment
ATWS	Anticipated Transient Without Scram
ASME	American Society of Mechanical Engineers
BPVC	Boiler Pressure Vessel Code
BOC	Beginning of Cycle
C/C	Carbon-Carbon composite
CAS	Chinese Academy of Science
CRADA	Cooperative Research and Development Agreement
CTE	coefficient of thermal expansion
CVD	chemical vapor deposition
CVI	chemical vapor infiltration
DOE	U.S. Department of Energy
dpa	displacements per atom
DRACS	direct reactor auxiliary cooling system
EDS	energy-dispersive x-ray spectroscopy
EPMA	electron probe microanalysis
FEM	Finite Element Methods
FFHR	Force-Free Helical Reactor
FHR	Fluoride salt–cooled High-temperature Reactor
FHR-DR	FHR Demonstration Reactor
FLiBe	generally 67LiF-33BeF_2 (mole percent)
FLiNaK	generally 46.5LiF-11.5NaF-42KF (mole percent)
GD-MS	Glow discharges mass spectroscopy
GI-XRD	grazing incidence x-ray diffraction
GT-MHR	Gas Turbine-Modular Helium Reactor
HTGR	High Temperature Gas Reactor
HTR	High Temperature Reactor
ICP-OES	inductively coupled plasma optical emission spectrometry
IHX	Intermediate Heat Exchanger
LFMSR	Liquid Fuel Molten Salt Reactor
LWR	Light Water Reactor
LOFC	Loss of Forced Convection
LS-VHTR	Liquid-Salt Very High Temperature Reactor
LUHS	Loss of Ultimate Heat Sink
MSBR	Molten Salt Breeder Reactor
MSR	Molten Salt Reactor
MSRE	Molten Salt Reactor Experiment
NACC	Nuclear Air Combined Cycle
NASA	National Aeronautics and Space Administration
NGNP	Next Generation Nuclear Plants
NITE	nano-infiltration and transient eutectic phase

NRC	US Nuclear Regulatory Commission
OES	optical emission spectrometry
ORNL	Oak Ridge National Laboratory
PBMR	Pebble Bed Modular Reactor
PLS	proportional limit stress
POF	probability of failure
PyC	Pyrolytic carbon
PRACS	primary reactor auxiliary cooling system
PWR	Pressurized Water Reactor
R&D	research and development
SEM	scanning electron microscopy
SiC	silicon carbide
SiC/SiC	silicon carbide/silicon carbide matrix composite
SINAP	Shanghai Institute of Applied Physics
Sm-AHTR	Small Modular AHTR
T	tritium
TAP	Transatomic Power
TDS	thermal desorption spectrometry
TF	tritium fluoride
TMSR-LF	Thorium Molten Salt Reactor–Liquid Fuel
TMSR-SF	Thorium Molten Salt Reactor–Solid Fuel
TRISO	tri-structural-isotropic
UFS	ultimate flexural strength
UTS	ultimate tensile strength
VHTR	Very High Temperature Reactor
WIC	Weak Interface Ceramic
WMC	Weak Matrix Ceramic
XPS	x-ray photoelectron spectroscopy
XRD	x-ray diffraction

EXECUTIVE SUMMARY

The purpose of this report is to identify the research and development (R&D) gaps for potential applications of silicon carbide/silicon carbide matrix (SiC/SiC) composite components for Generation IV Molten Salt Reactors (MSRs).

There are several different MSR concepts, which can be grouped into two classes: those with solid fuel and those with liquid fuel. The Fluoride salt-cooled High-temperature Reactor (FHR), with solid fuel and molten salt coolant, and the Liquid Fuel MSR (LFMSR), a reactor wherein the fuel is dissolved into the molten salt, are the example concepts in these two classes, respectively. The primary candidate coolant for FHRs is a molten fluoride salt; an LFMSR assumes the use of either fluoride or chloride salt mixtures. As a Generation IV reactor concept, MSRs shall demonstrate sustainability (mainly waste manageability), proliferation-resistant secure nuclear systems, competitive cost of energy, and safety and reliability, including acceptable performance of key materials for licensing.

The FHR concept is considered technologically more mature than other MSR concepts. FHRs typically have a thermal neutron spectrum, whereas other MSRs have been designed with epithermal or fast neutron spectra. Core outlet temperatures are in general below 750°C with pressures near atmospheric conditions. The FHRs feature high-temperature solid fuels, passive safety features such as auxiliary cooling systems like those in sodium fast reactors, intermediate heat exchangers, and salt freeze tanks.

SiC/SiC composites are particularly suitable for certain components in these systems because they have outstanding high-temperature capability and tolerance against neutron irradiation. Moreover, MSRs in general will greatly benefit from the use of SiC/SiC composites for components that need to withstand harsh operating environments combining some, or all, of the characteristics of high temperature, high neutron flux, high lifetime neutron fluence, and direct contact with molten salt, regardless of reactor concepts or designs. The materials and application technologies surrounding SiC/SiC composites are rapidly advancing as the material find niche, yet growing, applications—mainly outside the field of nuclear energy. However, significant R&D is still needed before SiC/SiC composite materials and their application technology become ready for the qualification of designs employing components made of these materials.

The purpose of this study is to identify the remaining technology gaps for SiC/SiC composite materials and to evaluate their readiness for use in MSRs with regard to aspects concerning the maturity of design methods and rules; the materials and manufacturing techniques, with a focus on limitations regarding scalability and component sizes; material performance, in terms of mechanical and thermal property data; and chemical interactions and compatibility.

Design Methodology

SiC/SiC composites have been identified as suitable materials for several MSR core components, which include, but are not limited to, the reactor control rod and fuel assembly supports, tie rod supports, core support plates, guide tubes for instrumentation sleeves, and the core barrel.

In general, components for fuel assemblies and reactivity control systems need to be evaluated for in-service conditions. Factors of critical concern include mechanical distortion due to radiation-induced warping, surface erosion and mechanical debonding.

For FHRs, external loads, due to flows, pressure differentials, buoyancy etc., are expected to be different than High Temperature Gas Reactor (HTGR) loads and will have to be considered during design to show that the structures maintain adequate levels of integrity through the design life. Effects like thermal striping and flow induced vibration are likely to be important in FHR designs while less significant to HTGR designs (because the salt is a better heat transfer material and more dense than helium). The ASME code would

need to be reviewed to ensure that it makes sufficient provision to address these effects. It also need to be compared with load conditions expected for LFMSRs.

The design rules for high-temperature reactor composite core components are near completion for first publication in the ASME Boiler and Pressure Vessel Code Section III Div. 5 code. It makes provisions for HTGRs as well as MSRs, specifically FHRs. Future compatibility assessment for LFMSRs may be required as the different front runner technologies advance.

The design rules need to be validated by the US Nuclear Regulatory Commission (NRC) before it can endorse the code for licensing purposes. Due to the lack of a demonstration reactor and a need to validate the rules, it is required to develop a technical basis document that supports the conditions described in the code with benchmarking data.

The establishment of standard material specifications, test methods, and practices is an important part of the design rules development. The currently available test standards, are missing some of the important elements required for qualifying SiC/SiC component designs for MSRs, in particular, in the area of test methods for elevated temperature properties. In addition, many test standards developed in ASTM Committee C28 on Advanced Ceramics are missing the section on precision and bias based on the round-robin testing campaigns.

Current experience with SiC/SiC composites use in jet engines and the ongoing development of SiC/SiC technologies for accident-tolerant light water reactor (LWR) fuels are expected to advance the technological maturity of SiC/SiC composites as structural components of nuclear reactors. This is of critical importance because SiC/SiC composites have much less structural application experience and fewer data compared with metals. Interactions with these developments are essential in advancing the design methodology related to SiC/SiC for MSRs.

Materials and Manufacturing

SiC materials of interest for nuclear structural applications are mostly continuous fiber-reinforced ceramic matrix composites, which consist of SiC fiber, SiC matrix, and the fiber-matrix interphase. Nuclear-grade composites consist specifically of fully crystalline and stoichiometric SiC fibers and matrices and use a carbon interphase. Such composites are available through the chemical vapor infiltration (CVI) and nano-infiltration and transient eutectic-phase (NITE) processing routes.

Fabrication of large and complex-shape components made of nuclear-grade SiC/SiC composites will be necessary for MSR applications. Although processing elements—such as the fiber preforming process, matrix densification, and joining/integration technologies—are reasonably mature, demonstration of the component fabrication and performance against the design requirements will be required.

Assembly technology for both CVI and NITE SiC/SiC composites exists, and it enables the fabrication of complex components made without using exotic joining materials. Testing was performed on the strength of SiC-to-SiC joints, and retention of joint strength following irradiation was demonstrated for a SiC-based bonding layer. However, because joints are often the weakest links in components and systems, they will have to be further evaluated.

Fabrication technologies for dissimilar joints were demonstrated for SiC joined to limited metallic materials, including aluminum and steels. Such technology development often involves significant challenges. Common hurdles at elevated temperatures are undesirable reactions and residual stresses. Further development of joining technology will be required if joining SiC to dissimilar materials is required for MSR applications.

Securing gas-tightness proved to be a significant challenge in the development of LWR fuel cladding, for both as-fabricated SiC/SiC composite tubes and end-plug joints. If hermeticity is required for SiC/SiC components for MSRs, manufacturing technologies to ensure it need to be fully developed and demonstrated for the composites and the integration elements. For MSRs, particularly the liquid fuel concepts, molten salt ingress into open pores and cracks exposed to the outer surfaces may present an important concern. Manufacturing of SiC/SiC composite components will have to address such concerns.

Properties and Radiation Effects

The design database for key physical, thermal, and mechanical properties is rapidly being augmented for CVI SiC/SiC composites as the R&D toward LWR applications progresses. However, a significant knowledge gap will remain, primarily in the areas related to the high-temperature operation of MSRs and the molten salt–specific operating environment, even after the ongoing LWR accident-tolerant fuel technology development effort successfully accomplishes its mission.

The primary gap in the thermo-mechanical properties and performance include those related to the component service life, including creep, fatigue, and environmentally assisted mechanical degradation. In particular, stress-corrosion cracking and the resultant slow crack growth could be a critical design-limiting issue. Moreover, understanding of the effects of repetitive motion, such as fatigue and fretting, in the salt environment needs to be established because they are important for MSR applications.

The other major gap in this category is an understanding of irradiation effects on mechanical properties. The effects of neutron irradiation on mechanical properties can be a significant design-limiting issue for SiC/SiC components when the expected neutron dose is very high. In fact, recent studies indicate significant strength degradation after ~70 dpa irradiation in a 500–800°C temperature range because of the radiation instability of Hi-Nicalon Type S fibers and the carbon interphase.

For improved high-dose irradiation tolerance, true SiC fiber (free of significant second phases or off-stoichiometry) and improved interphase materials or designs will be needed. Although such developments are currently being undertaken or proposed, none of them is ready for industrial-scale production. SiC/SiC composites made of improved radiation resistance constituents are anticipated to be resistant to very high-dose irradiation, potentially offering a material solution for the fast spectrum MSR concepts where the core materials receive very high doses of neutrons, whereas the present generation SiC/SiC composites may present adequate radiation stability for thermal spectrum MSR concepts where the neutron dose to core materials will be moderate.

Chemical Compatibility

SiC components will be exposed to diverse chemical environments. In FHRs, the environment will include metals, carbon, impurities, and transmutants in a molten fluoride salt. A preferred salt for the FHR's primary coolant system is 67LiF-33BeF_2 (FLiBe), which is also a candidate for the intermediate loop system, along with 46.5LiF-11.5NaF-42KF (FLiNaK). Suspected incompatibility with chloride salts needs to be verified.

The corrosion of SiC in molten fluoride salts is driven by thermal gradients and salt impurities. SiC exhibits wettability and chemical reactivity with liquid metals but is generally stable in molten fluoride salts so long as the salt purity is maintained. Very little is known about thermal gradient–driven corrosion which is likely to sustain corrosion. The corrosion of SiC in molten fluoride salt depends directly on the redox condition of the salt and the various methods used to mitigate impurities and tritium. The corrosion of SiC in FLiBe and FLiNaK has been studied directly in very few instances, whereas the corrosion of carbon and heat exchanger alloys in molten fluoride salts and nitrate salts is more well known. SiC/SiC components are proposed in areas of higher neutron fluxes and should be considered permanent installations in the reactor core. Replacement would be costly and could require prolonged shutdown periods.

Tritium is a major issue for FHRs. Recent studies have modeled the tritium levels in FHRs and predict that it will exceed those in heavy water reactors at equilibrium conditions. The corrosion behavior of SiC and container alloys is directly related to the tritium capture and recovery systems. Hydrogen and its isotopes are highly mobile in metals and possibly in SiC. Solubility of tritium and lattice diffusion behavior in irradiated SiC should be studied in conjunction with the surface corrosion and microcracking.

Corrosion testing can be performed with static experiments in sealed capsules or dynamic loop experiments (thermal or forced convection). Historically, most of the loop testing of alloys in molten fluoride salt occurred at Oak Ridge National Laboratory in the 1970s and 1980s. There is not a lot of theoretical development in this area of science, and much of the research is very much applied R&D. The static tests have demonstrated their practicality, but they are prone to error; and oxygen leaks could cause a much higher corrosion rate. Thermal and forced convection loop corrosion testing of SiC has not yet been performed.

The corrosion resistance of SiC and variants in molten fluoride salts will depend on the redox condition of the salt and tritium capture and salt purification methods. Measurements of equilibria and thermochemical data are needed, and predictions of corrosion reactions, corrosion products, and kinetics to determine the corrosion behavior of SiC in the molten fluoride salts FliBe and FliNaK. With thermochemical measurements and thermodynamic calculations, the control/removal of impurities can then be validated by experiment. Kinetic measurements and rate equations can then follow to develop predictive models.

ACKNOWLEDGMENTS

Support for this research was provided by the US Department of Energy, Office of Nuclear Energy (DOE-NE), Advanced Reactor Technologies program, for the completion of activity milestone M3NT-18OR070502012. Oak Ridge National Laboratory is managed by UT-Battelle LLC under contract no. DE-AC05-00OR22725 for the US Department of Energy.

The authors extend their appreciation to Dr. Lou Qualls, Dr. David Holcomb, Dr. Stephen Raiman, Dr. Tim Burchell, Dr. Cristian Contescu, Dr. Steven Gonczy, Dr. Michael Jenkins, Dr. Lauren Garrison, and Mr. Mark Mitchell for their input and technical review.

1. INTRODUCTION

The purpose of this report is to survey the literature and identify the key research and development (R&D) gaps regarding the application of silicon carbide/silicon carbide matrix (SiC/SiC) composites for structural components of a molten salt reactor (MSR). SiC/SiC materials of interest for nuclear structural applications are mostly continuous fiber reinforced ceramics matrix composites, which consist of a SiC fiber (like High Nicalon Type S, Tyranno SA3 and Sylramic), SiC matrix (like the chemical vapor infiltration (CVI) matrix or the Nano-Infiltration and Transient Eutectic phase (NITE) matrix), and a carbon interface between the fiber and matrix (such as the multilayer pyarolytic carbon (PyC)/SiC interfaces).

In general, there are distinct differentiations between two MSR technologies; the fluoride-cooled high-temperature reactors (FHRs) with solid fuel and a "clean" (non-fuel) salt coolant, and the liquid fuel MSR (LFMSR) in which the coolant also carries dissolved fissile material and fission products. Both reactor technologies are considered in this report.

Historical feasibility issues identified for SiC/SiC components have included (1) corrosion of SiC in the candidate liquid salts, (2) high-dose neutron radiation effects, (3) static fatigue failure of SiC/SiC, (4) long-term radiation effects including irradiation creep and radiation-enhanced static fatigue, and (5) the fabrication technology for the hermetic wall and sealing end caps [1]. As a result, recent SiC/SiC R&D related to MSRs has focused on (1) thermodynamic analysis and experimental examination of SiC corrosion in candidate liquid salts, (2) assessment of long-term mechanical integrity issues, and (3) assessment of high-dose radiation effects relevant to the anticipated operating conditions.

Early MSR designs often used Hastelloy N (a nickel-based metal alloy) and graphite as the structural and core components, respectively. Both Hastelloy and carbon-based materials have their own unique challenges in the MSR environment. SiC/SiC composites are particularly suitable for certain in-core mechanical structures because of their outstanding high temperature capability related to thermal conductivity and mechanical strength and then its tolerance against neutron irradiation. Therefore, SiC/SiC is a potential replacement for several reactor core components currently designed for Hastelloy N or even carbon/carbon components. Additionally, the long-term corrosion effects on metal components such as instrumentation, reactivity control, and reactor enclosure are still serious concerns for MSRs [2]. If SiC/SiC can withstand salt exposure with limited corrosion, it has been proposed that SiC/SiC composites be used as a coating or barrier to protect the metal components from the salt at high temperatures, which would be advantageous for both FHR and LFMSR development. This report discusses the progress made on these issues.

The purpose of this study is to investigate and identify the remaining technology gaps for SiC/SiC composite materials and to evaluate the material readiness on aspects concerning the

- maturity of design methods and rules needed to design reactor core components
- materials and manufacturing constraints and techniques, with a focus on limitations regarding scalability and component sizes
- material performance under irradiation and in corrosive environments, assessing mechanical and thermal property data
- chemical interactions and compatibility

This report makes initial recommendations on a path to continue the development of SiC composites for applications in FHR and MSR components.

2. DESIGN METHODOLOGY

2.1 TYPES OF REACTORS AND DESIGN MATURITY

Historically there were two iconic MSRs, the Aircraft Reactor Experiment (ARE) and the Molten Salt Reactor Experiment (MSRE), both designed by Oak Ridge National Laboratory (ORNL) in the mid-1900s. They operated for a total of 100 hours and 21,000 hours, respectively. Between the mid-century era and today, the development strategy and motivation for the development of MSRs continues mostly as an international effort and by private companies, but with added awareness of the increased safety benefits of such systems and the growing demand for energy. Representative FHR concepts are the Liquid-Salt Very High Temperature Reactor (LS-VHTR) or the earlier Advanced High Temperature Reactor (AHTR) during its preconceptual phase.

There are more than the two main technologies, FHR and LFMSR, as defined in this report [3]; but the scope discussed herein mostly concerns the two main technology groups, with an emphasis on FHRs. Recently, the pebble-bed FHR has been of interest with Kairos Power, a US-based company that announced plans to commercialize its FHR within the next decade. The Kairos FHR will be designed to harvest nuclear heat in a Nuclear Air Combined Cycle (NACC) that uses a conventional natural gas turbine modified to accept nuclear heat. This design can co-fire natural gas to meet peak power demands and supplement the natural gas market. The FHR is cooled with clean molten fluoride salt, moderated by graphite, and uses encapsulated fuel particles similarly to a high temperature gas-cooled reactor (HTGR). The FHR concept is probably the nearer-term MSR option that focuses on demonstrating acceptable performance of key materials for licensing [1,3,4]. Typical core structural materials in contact with the salt coolant include graphite, SiC, and nickel-based alloys [2,5].

Various FHR technology concepts exist, such as the AHTR, the Small Modular AHTR (Sm-AHTR), the Pebble Bed-AHTR (PB-AHTR) or "Mark 1" [6], and the Thorium Molten Salt Reactor Solid Fuel (TMSR-SF). The Mark 1 concept was originally developed by University of California–Berkeley and is the basic concept on which the forerunner for the most near-term US technology is based. The TMSR-SF is also a pebble bed reactor, developed by SINAP in China; and similar to the TMSR-LF (which uses liquid fuel), it has a three-stage development plan from simulator to demonstration [7].

In the other main MSR category, the LFMSR, the fuel is dissolved in the salt, which is circulated through the primary heat transfer loop. Several thermal and fast spectrum LFMSR designs are being pursued commercially. Some of the fast spectrum versions make the LFMSR promising for breeding or high-conversion options. Development is largely driven by private investors (both US and non-US companies), such as Terrestrial Energy (thermal burner using uranium) and Transatomic Power (hybrid burner using uranium). Other companies developing LFMSRs include TerraPower (fast breeder using uranium), ThorCon (thermal burner using thorium), Flibe Energy (thermal breeder using thorium), and Elysium Industries (fast breeder using uranium). Several other design concepts are in development internationally, such as the Moltex (UK), Seaborg Technologies (Denmark), and FuJi (Japan) [8-11].

There are various coolant salt applications and design considerations. Typically, there are two to three heat transfer loops: the fuel salt loop; the primary coolant loop; and the intermediate or secondary coolant loop and/or the power generation loop, which assumes either a Brayton cycle (gas) or a Rankine cycle (steam). The work discussed in this report is primarily concerned with the coolant and material components associated with the reactor core as part of the fuel salt or primary coolant loop. Table 2.1 shows some major design concepts and their respective design parameters. The data set from the public domain is limited but is listed to explore the design space options.

Table 2.1. MSR reactor types and properties.

Design	FHR-DR	AHTR	Sm-AHTR	Mark 1	TMSR-SF1	TMSR-LF1	IMSR	TAP
Design authority	ORNL	ORNL	ORNL	UCB	CAS (SINAP)	CAS (SINAP)	Terrestrial Energy	Trans-atomic Power
Type	FHR	FHR	FHR	FHR	FHR	LFMSR	LFMSR	LFMSR
Neutron spectrum	Thermal	Thermal	Thermal	Thermal	Thermal	Thermal	Thermal	Thermal/ epithermal
Fuel type	Solid – prismatic block	Solid – prismatic block	Solid – prismatic block	Solid – pebble bed	Solid – pebble bed	Liquid fluoride fuel salt	Liquid fluoride fuel salt	Liquid fluoride fuel salt
Coolant	2LiF-BeF_2, (FLiBe)	FLiBe	LiF-BeF_2	Flibe ($7Li_2BeF_4$	FLiBe	LiF-BeF_2 -UF_4 -ThF_4	–	LiF-(Act)F4]
Moderator	Graphite	Graphite	Graphite	Graphite	Graphite	Graphite	Graphite	Zirconium hydride ($ZrH_{1.66}$)
Power [MW_t]	100	3400	125	236	10	2	400	1250
Core diameter [m]	~3.8	~9.6	3.0	–	2.85	–	–	–
Core height [m]	~ 3.7	6	4.0	2.5	3.00	–	–	–
Vessel diameter [m]	~4.4	10.5	3.5	3.5	3.05 (reflector)	–	3.5	–
Vessel height [m]	~9.5	19.1	9.0	12.0	7.84 (reflector)	–	7.0	–
Core design temperatures [°C]	700	700	650–700	700	600– 700	650	700	650
Max fuel temp. [°C]	970	837	–	900	1400	–	–	–
Fuel residence period [months]	–	12	6	16	6–8	–	84	–
Fast flux [n/cm2.s], [E > 0.1MeV]	–	6.18×10^{13}	–	6.95×10^{13}	3.5×10^{14}	–	–	–
Design life [years]	–	60		60	20	–	60	–

Table 2.1 lists and Figure 2.1 shows some of the MSRs that have a thermal neutron spectrum and are similar to HTGRs, such as the Gas Turbine–Modular Helium Reactor (GT-MHR). Transatomic Power is developing the TAP liquid fuel MSR, which uses a LiF-based fuel salt and a zirconium hydride moderator. It is designed for a thermal/epithermal (1 eV–1 MeV) neutron spectrum (Figure 2.2). Not included are examples of fast spectrum reactors like those from TerraPower and Elysium Industries. Fast spectrum reactors are inclined to use chloride-based fuel salt, and compatibility with SiC needs to be verified. In general, LFMSRs have higher fluences, which may be more limiting on component life and require greater chemical stability through redox control. All designs have theoretical core outlet temperatures below 750°C and a variety of neutron spectra (thermal, epithermal, and fast) using graphite and zirconium hydride as a moderator, or no moderator, as in the case of fast spectrum reactors.

Most of the reactors have an average thermal neutron flux greater than 10^{14} $s^{-1}cm^{-2}$ [12].

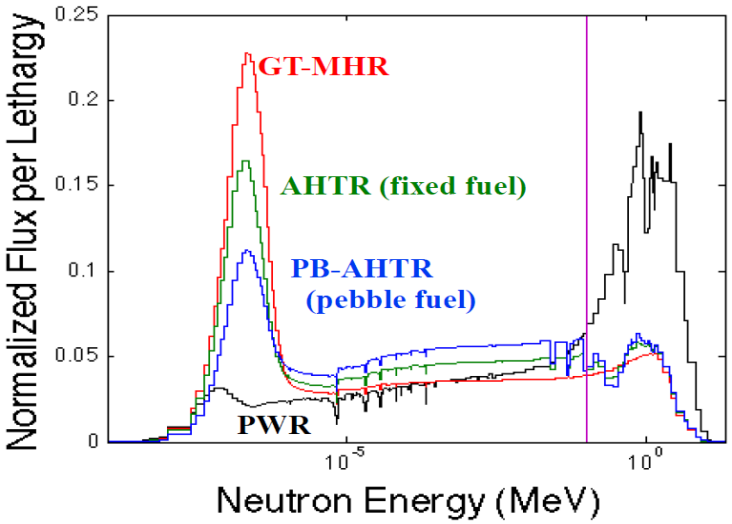

Figure 2.1. Comparative neutron flux spectra normalized to neutron energy between the AHTR, GT-MHR, PB-AHTR, and a pressurized water reactor [PWR]. [13]

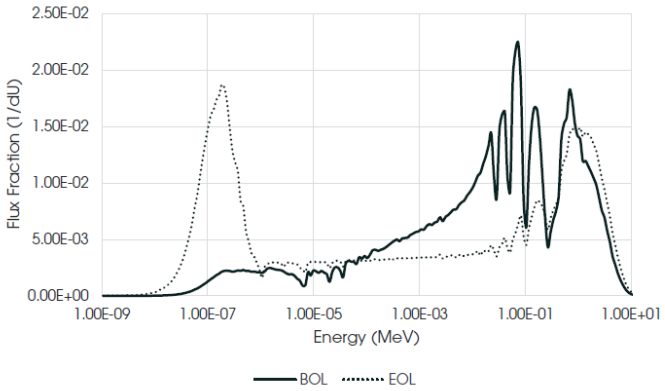

Figure 2.2. Neutron spectrum in a zirconium hydride–moderated TAP LFMSR at the beginning and end of life. [14]

Passive safety is one of the most marketable features of MSRs. Past experience with fast reactors and breeder reactors, has demonstrated inherent safety features in the design, such as a closed primary circuit, salt freeze tanks, intermediate heat exchanger (IHX), and modular decay heat rejection using the accident-ready primary reactor auxiliary control system (PRACS) and direct reactor auxiliary cooling system (DRACS) [15]. The PRACS is designed to match the decay heat for the first 1–2 hours of a Loss of Forced Convection (LOFC) accident, and the DRACS for the first 1–2 days. The DRACS is entirely buoyancy driven. The IHX has the advantage of minimizing the impact of an accident or a loop break in the primary system that affects the secondary system. In a Loss of Ultimate Heat Sink (LUHS) accident scenario, the intermediate loop cooling is lost and the reactor scrams. As the temperature of the core rises, the fission in the fuel ceases as a result of resonance broadening (Doppler effect), which is a strongly negative fuel temperature reactivity feedback. An LOFC accident scenario is similar, in that—the reactor protection system detects an off-normal condition and the reactor scrams.

The LOFC and LUHS scenarios are severe accidents with low probability. After an LOFC or LUHS scenario has occurred, a worst-case accident scenario is the anticipated transient without scram scenario, in which the reactor scram system fails to respond. Simplified calculations predict that the coolant will equilibrate near the original fuel temperature, below 800°C, well below the coolant boiling point of about 1430°C (for FLiBe). The system response and reliability in these scenarios should be carefully demonstrated.

2.2 TYPICAL APPLICATIONS FOR SIC COMPONENTS, FUNCTION, GENERAL REQUIREMENTS, AND REACTOR LOCATION

Ceramic composite materials like SiC/SiC and carbon/carbon (C/C) composites are candidate structural materials for use in nuclear reactor cores. Characteristics like high-temperature stability, oxidation and corrosion resistance, and radiation tolerance make ceramic composites more attractive than other high-temperature structural metals. Possible near-term uses for SiC/SiC reactor components in solid fuel applications include

- Control or tie rod supports (block and pebble fuel types)
- Core support plates or fuel salt distribution plates (block and pebble fuel types)
- Core barrel (block and pebble fuel types)
- Fuel and control blade assembly supports (block fuel types)
- Reactor core supports (block and pebble fuel types)
- Possible replacement for the C/C guide tubes and fuel assembly mechanical structure (block and pebble fuel types)
- Instrumentation sleeves or other barriers between metal and salt for high temperature interaction. (block and pebble fuel types)
- Wetted refueling mechanisms

For liquid fuel applications, it is foreseen that SiC/SiC fiber composites can replace some primary loop components currently identified for nickel-based alloys. The SiC/SiC composites are both corrosion tolerant and approved for high-temperature nuclear applications under the ASME Boiler and Pressure Vessel Code (BPVC) Section III. These components can include primary loop piping, reactor vessel, valves, pumps, and heat exchangers [14]. In a pebble fuel, a chemical vapor deposition (CVD) SiC layer ensures the structural integrity of the particle under constant pressure and helps to retain fission products. In the case of zirconium hydride–moderator reactors, the material hermeticity properties will be significant in the event of hydrogen outgassing [16]. CVD SiC in the fuel and SiC/SiC composites for structural materials should be analyzed separately, although the latter is the focus of this report.

SiC/SiC may be more appropriate for reactor component design because of its greater toughness and its lower strength sensitivity compared to C/C as shown in Figure 2.3. Both SiC/SiC and C/C composites have less than ideal properties, but SiC/SiC tends to be more predictable. SiC/SiC material is anisotropic and the material fabrication process is standardized. In general, SiC/SiC composites use more expensive materials than C/C, but SiC/SiC has much higher neutron dose limits; and, depending on the operating conditions, it is possible that it can replace C/C components.

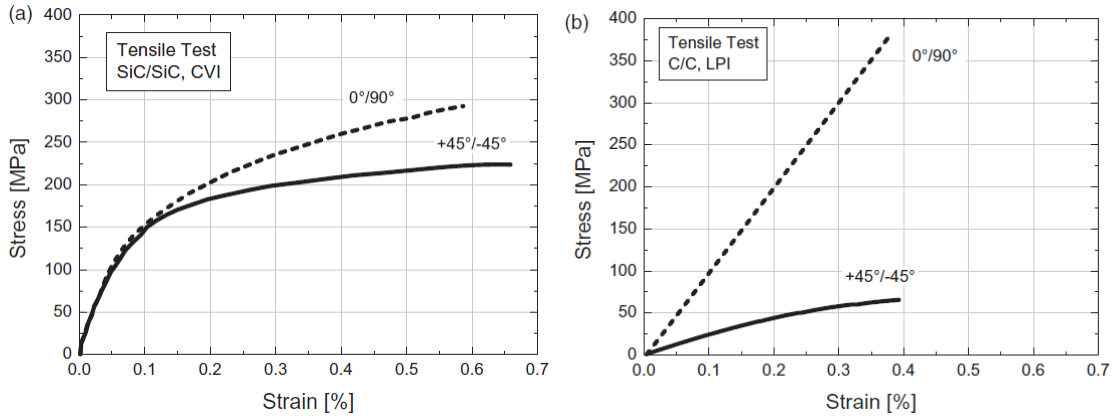

Figure 2.3. Stress-strain curves for (a) weak interface ceramics (SiC/SiC) and (b) weak matrix ceramics (C/C) composites. [17]

For feasible design considerations, the use of composite components as core supports requires that the composite components outperform the graphite core blocks with regard to operational life for radiation damage. Other applications may include the replacement of pump impellers or heat exchangers for classical design reasons (improved performance) at higher temperatures, above 850°C [18].

The FHR-demonstration reactor (FHR-DR) core within the vessel, illustrated in Figure 2.4, shows the early design concept. It proposes a prismatic block fuel design with integral fuel compacts and coolant channels. Design parameters are based on current HTGR experience. In total, the core dimensions are 3.6 m height and 3.24 m width. The fueled height of the core is approximately 2.61 m. The FHR-DR reactor is provided for point design criteria and used input from HTGR layouts [19].

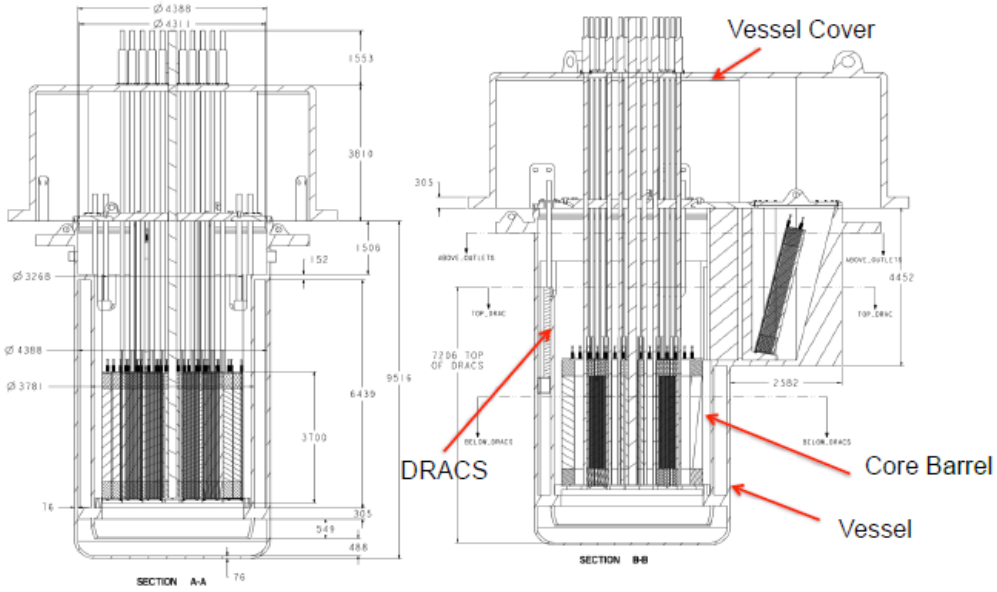

Figure 2.4. Elevation view of the FHR-DR showing the reactor core within the vessel. [19]

In the Sm-AHTR, two core variants are proposed in which SiC composites are likely to be used. For the annular cylindrical fuel option, the fuel is configured into annular compacts that are strung along composite vertical tie rods. A tie rod has a radius of 0.5 cm inside a hexagonal fuel block about 80 cm tall, as shown in Figure 2.5.

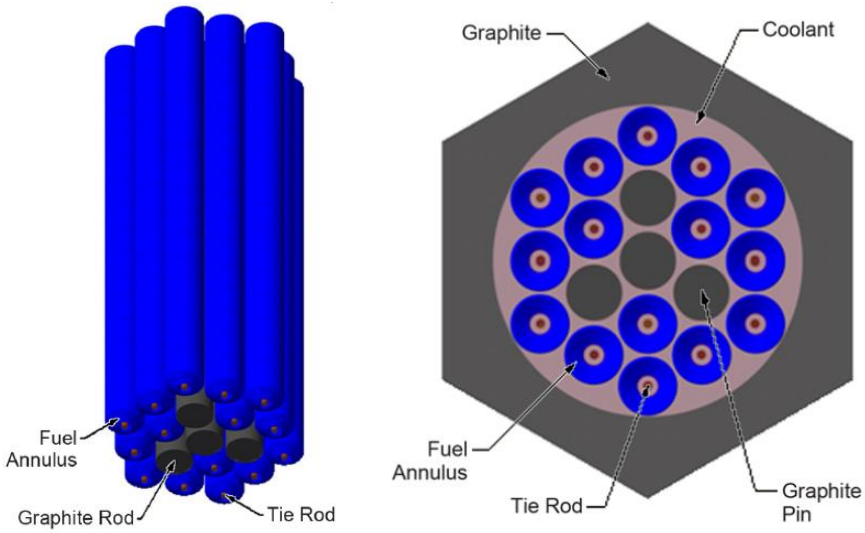

Figure 2.5. The Sm-AHTR annular cylindrical fuel option fuel bundle isometric and cross section view with the graphite channel. [18].

The other core variant design of the Sm-AHTR is where the fuel is configured into core planks (honeycomb structure) that are mounted into a composite frame. The plank fuel bundle is 45 cm across the flats and the fuel block height is similar to that of the annular cylindrical fuel option. The dimensions and cross section are shown in Figure 2.6. The "Y" support structure shown in Figure 2.7, was originally proposed for C/C

composites, but for the reasons discussed previously, these structures can be produced as SiC/SiC composites. SiC/SiC composite sheaths connect the bottom and top honeycomb structure. For the Sm-AHTR "Y" plate design, the peak fuel temperature in the core will not exceed 1250°C during normal operations. Bypass coolant can be mixed with the core outlet flow to maintain the coolant temperature for the metal structures. From a steady state thermal hydraulic comparison study with reasonable variance in the coolant flow through the core, the maximum coolant temperature, on these type fuel designs, was below 720°C. For this scenario the coolant temperatures at the lower plenum and at the top plenum will be 650°C and 700°C respectively.

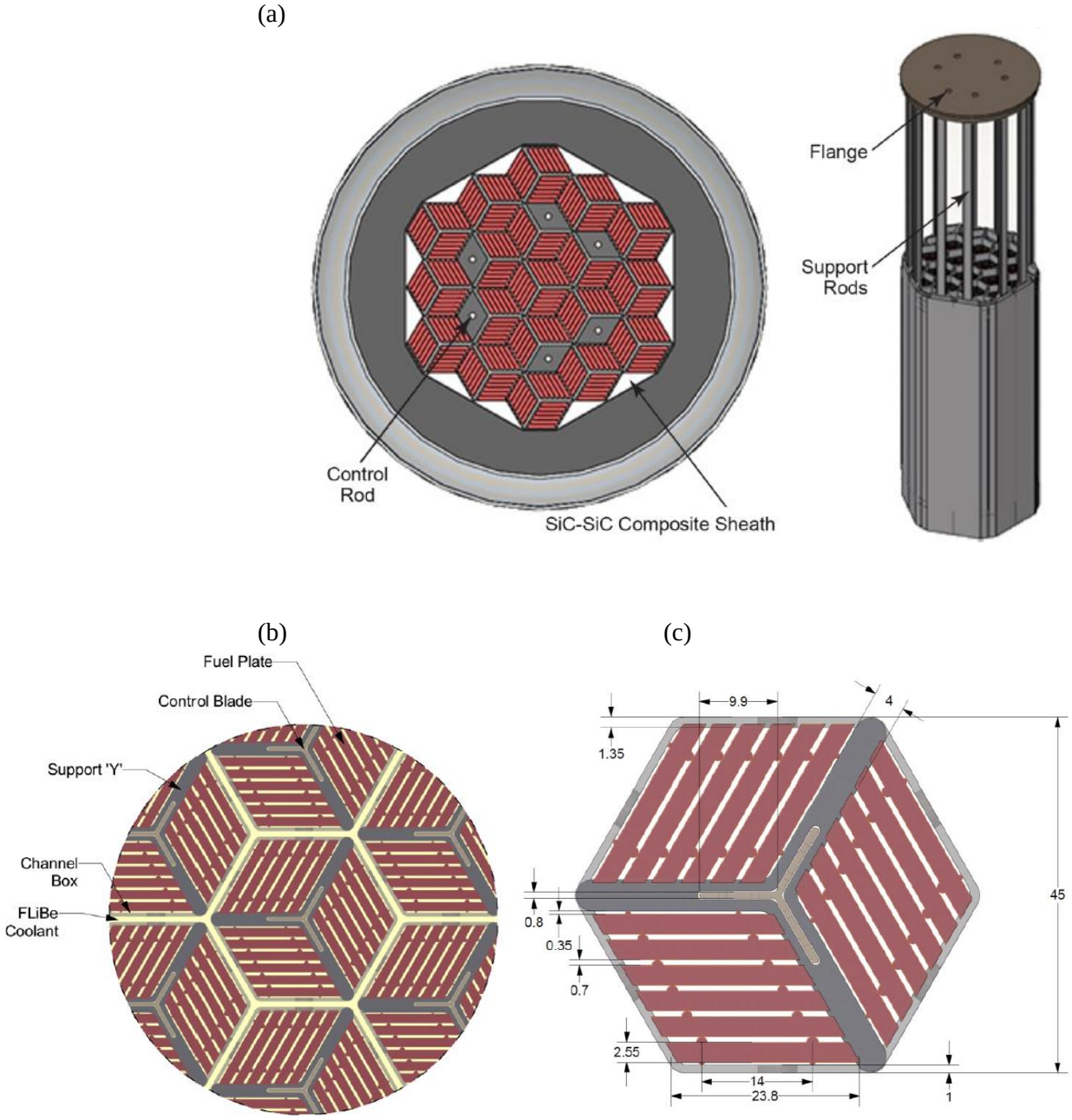

Figure 2.6. The Sm-AHTR and AHTR fuel assembly designs. (a) The Sm-AHTR plank-fuel-assembly cross section and removable core subassembly [18], (b) The AHTR plank fuel reference design assemblies detail and (c) associated dimensions [20].

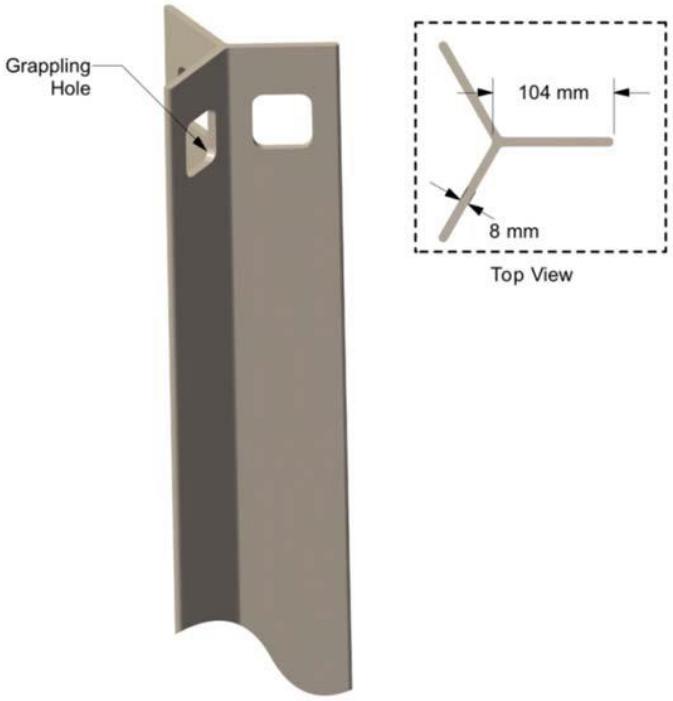

Figure 2.7. Top portion of the AHTR control blade. [20]

The plank fuel assembly option was also the proposed core reference for the AHTR. Its geometric characteristics are given in Table 2.2.

Table 2.2. Main geometric characteristics of the fuel assembly for the reference AHTR design. [20]

Characteristic	**Value (cm)**
Total height	600
Fueled region height	550
Channel box wall thickness	1
Y-shape thickness	4
Coolant thickness between plates	7
Control blade location thickness	1
Control blade location wing length	10

The Sm-AHTR concept considered a salt-salt Hastelloy-N heat exchanger with a shell-and-tube type countercurrent flow design with ~1,416 tubes, and typical outer diameter dimensions of ~25.4 mm, thickness of ~ 1.6 mm, and effective length of about ~2 m. Replacing Hastelloy-N with SiC/SiC composites is an option suggested as a design development strategy for reactor internals or heat exchangers, that need to operate at coolant temperatures above 850°C [18].

For the TMSR-SF model, the core region is an octagonal prism with two regions: a central control system channel zone and a fuel pebble zone, as shown in Figure 2.8. For comparison, the core region is 1.386 m high, and a central control rod channel is a square 0.35 m long and wide. Typical control rod tube dimensions for the TMSR-SF are ~2.5 m in height and between ~55 mm for the inner diameter and

~110 mm for the outer diameter, with a small gap (~0.5 mm) for thermal deformation. The control support plates are between ~2.8 m and 3.0 m in diameter and ~0.8 m thick [21].

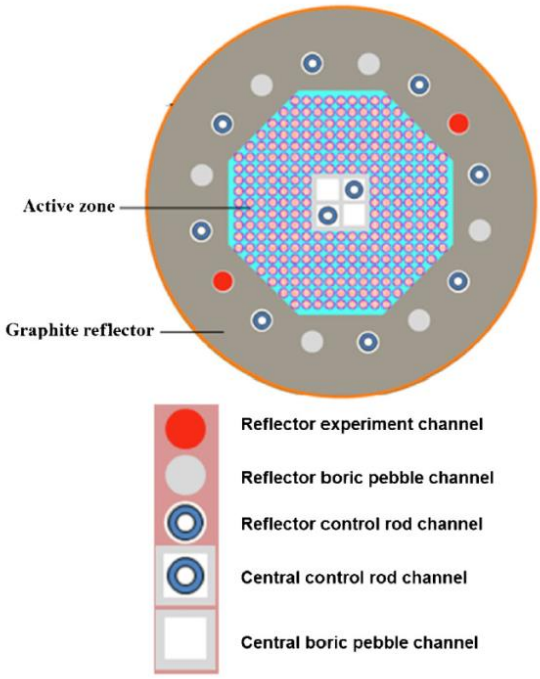

Figure 2.8. TMSR-SF cross-sectional view. [21]

Figure 2.9 shows the layout of the AHTR core and indicates the regions of the core barrel as well as the lower support plate. The core is 9.56 m in diameter and the fueled region is 7.81 m. The core barrel is a 2 cm thick liner between the radial reflector and the fueled core regions. The height of the core is ~6 m.

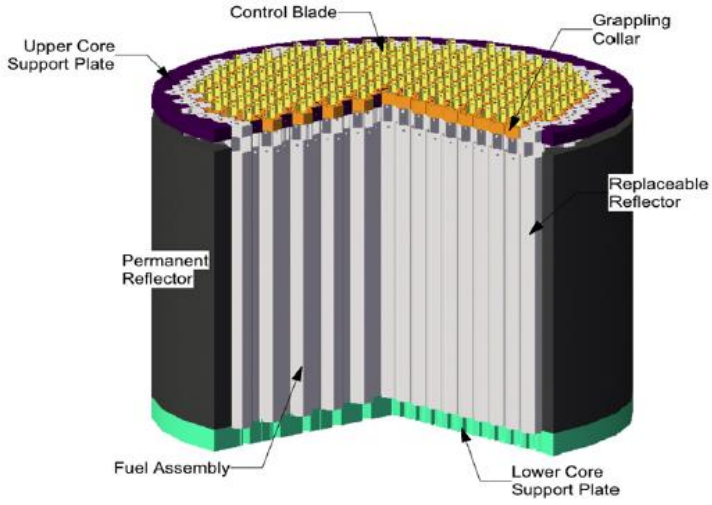

(a)

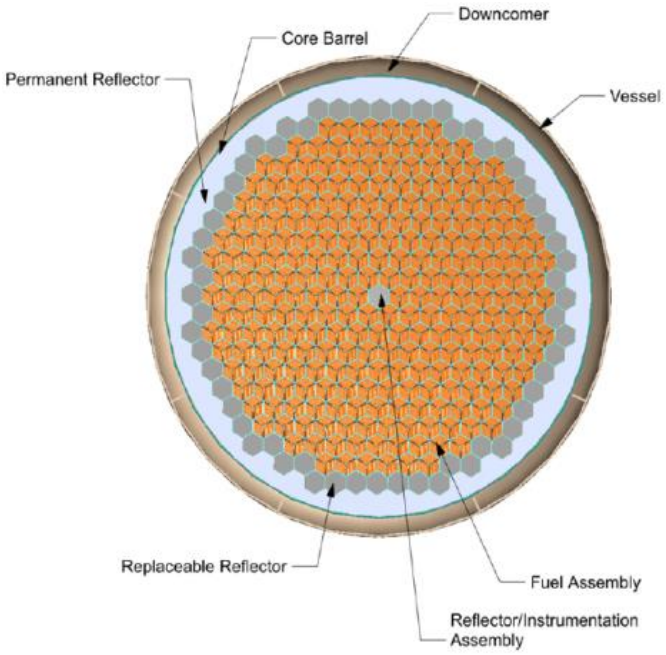

(b)

Figure 2.9. AHTR reference core. (a) isometric view and (b) cross section view [22].

2.3 TYPICAL TEMPERATURES, FLUENCE, AND LOADING CONDITIONS

The typical temperatures, fluences, and loading conditions listed in Table 2.1 are associated with reactor vessel internals, which include the upper and lower core support plates, mounting struts and sliding mounts, fuel assembly headpiece, control blade guide tubes and rods, and core barrel. For typical solid-fuel FHRs like the AHTR, the SiC/SiC components are not required to be hermetic [20].

A preconceptual design study for the FHR-DR of the core design and safety analysis, described in [23], provides initial temperature and fluence values for the operational conditions; it is shown in Figure 2.10.

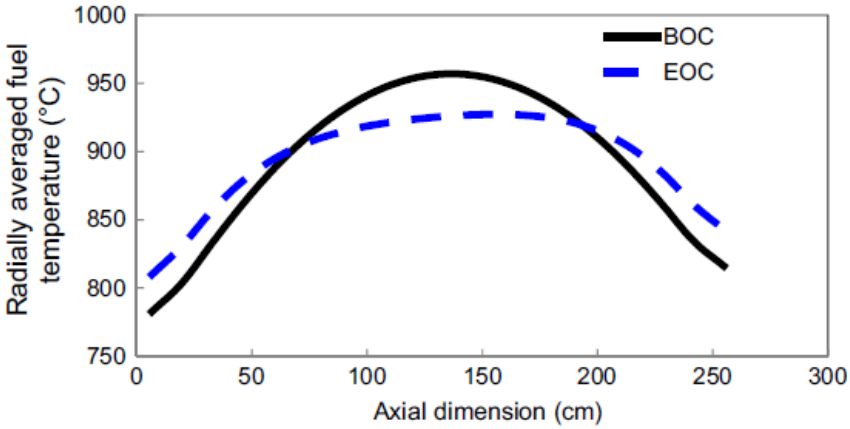

Figure 2.10. FHR-DR radial averaged fuel temperature. [23]

Thermal conductivity in the fueled region changes as a result of fission product buildup (inside the fuel kernels) and radiation damage. Fuel temperature increases as the fueled thermal conductivity decreases, as has been modeled in the AHTR reference core design (Figure 2.11). The thermal conductivity change in the carbon matrix sleeve impacts the fuel temperature to a lesser extent with decreasing thickness. These fuel temperatures should not be significantly affected by replacing the C/C composites with SiC/SiC composites.

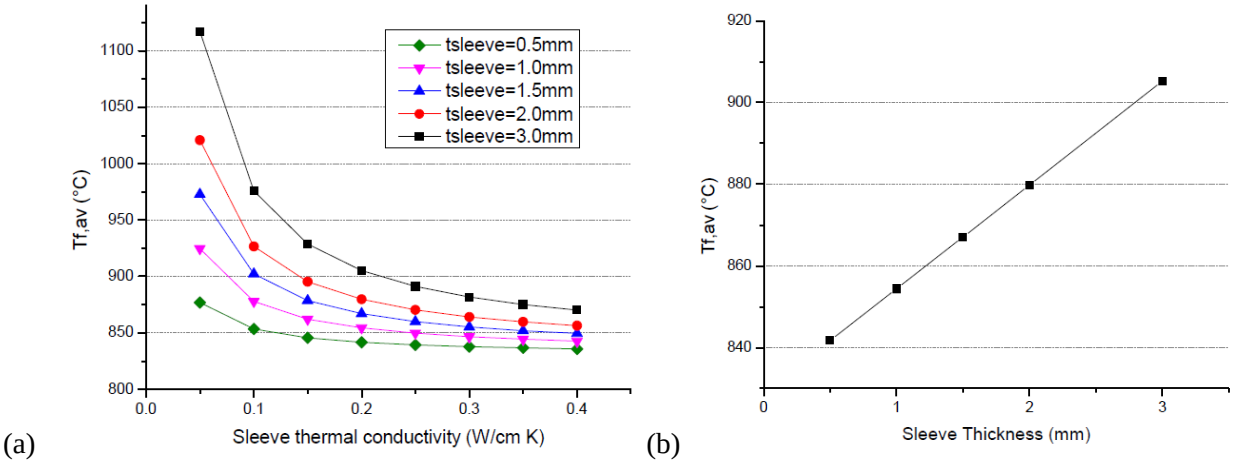

Figure 2.11. The AHTR reference core modelled fuel temperatures. (a) Maximum fuel temperature for the average assembly for different fuel sleeve thicknesses and (b) maximum fuel temperature dependence on sleeve thickness. [19]

The fast fluence determines the lifetimes of the materials within the core. In the AHTR reference design, the average fast fluence at the region of the core barrel is 5.7×10^{18} n/cm^2 with a total fast fluence of 4.8×10^{20} n/cm^2 over a planned 60-year period. Figure 2.12 shows the distribution of the fast neutron flux (E>50 keV) in the reactor core. The maximum fast flux for the central region is 0.19×10^{22} n/cm^2/year.

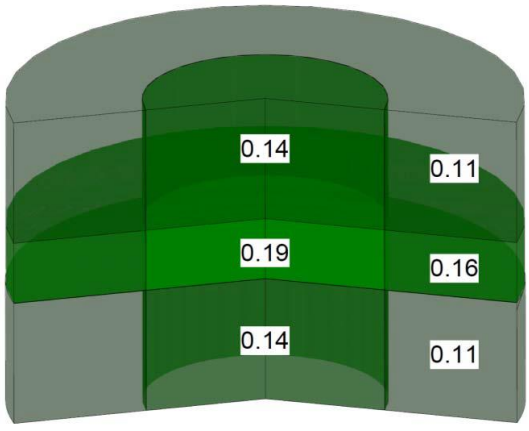

Figure 2.12. Region wise fast flux (E >50 keV) in the AHTR reference core at beginning of cycle ($\times 10^{22}$ n/cm^2/year). [20]

SiC/SiC provides a unique combination of high strength and thermal conductivity at high temperatures, as well as radiation tolerance, which makes it a good candidate for in-core mechanical structures. The structural elements in the reactor core require both tensile strength and fracture toughness/damage tolerance.

Compared with HTGRs, the reflector regions may be subject to much higher neutron dose rates and the chemical environment is very different. In general, the fuel operating temperature of FHRs peak at lower temperatures but have a higher peak in power levels.

Fuel and control rod and/or sleeve assemblies need to be evaluated for in-service conditions. Factors of concern include mechanical distortion due to radiation-induced warping, surface erosion, and/or mechanical debonding. Tight fittings should be avoided to allow for radiation-induced stress relaxation due to radiation-induced dimensional changes. For the AHTR, a prismatic block fuel type reactor, fuel replacement is expected before achieving fast fluences of 4×10^{22} n/cm^2 (E > 50 keV) [20], however, this is not expected in the case of a fueled pebble bed reactor that replaces fuel continuously.

It is also possible that the design of the MSR may require consideration of additional load combinations beyond the scope of normal practice. For example, freezing of the salt may need to be considered as an unlikely transient event. [24]

2.4 CODE DEVELOPMENT ACTIVITIES FOR SiC STRUCTURAL MATERIALS

Code development and documentation for composite materials have made significant progress and are in the last stages of review before being published in the ASME BPVC Section III Division 5 under subsection HA subpart B ("General Requirements for Graphite and Composite Materials") and subsection HH subpart B ("Nonmetallic Core Support Structures - Ceramic Composite Components").

The ASME code has adopted the same reliability approach for composite materials that has been developed and defined for graphite components under Section III Division 5. It defines the structural reliability classes applicable to composite components and signifies mechanical reliability in terms of safety.

The ASME BPVC for composite components differs from the code for metallic components, because failure of composite components can't be expressed as the absence of cracks (as in the case of metals) to ensure absolute reliability. Because of their nature (as in the case of graphite), a probability of failure (POF) approach is applied for composite materials and components. The POF values are derived from the loadings on the composite core components and failure of material due to undetectable microstructural defects/cracks/flaws/porosity. Ultimately, it is up to the designer to evaluate the effects of cracking of components and ensure that the components and assembly are damage tolerant. In addition, environmental effects during operation - such as irradiation and chemical attack, salt infusion, fatigue, and slow crack growth of the material - are to be considered in the design. The design specification specifies the service levels, which relate to the service limits applicable and define the allowable POF and deformation or other design limits for each composite core component in the core assembly.

There are several conditions that contribute to the design loadings, but the designer is required to determine and specify the loadings, which, at a minimum include the temperature distribution, fast flux distribution, design pressure distribution, and mechanical loadings on the components. The assessment of the composite core components must include consideration of the effects of chemical attack (both thermal and radiolytic), irradiation, abrasion and erosion, fatigue, creep, and slow crack growth. Additional MSR specific loadings may be determined in the course of the plant design.

Because of the considerable design flexibility in the architecture, structure, and properties for SiC/SiC and C/C composites, the composite material would need to conform to the requirements of the materials specification/s in the construction specification developed by the designer. Each component will have a detailed specification for the loading conditions set out in the code.

Besides the physical and mechanical material properties required for design, the material specification incorporates the irradiation effects, which include

- dimensional change
- irradiation creep coefficient
- coefficient of thermal expansion
- tensile strength (ultimate and proportional limit values)
- elastic modulus
- thermal conductivity

For the evaluation of chemical conditions, the material specification also requires as a minimum

- tensile strength (ultimate and proportional limit values)
- elastic modulus (dynamic)
- thermal conductivity

The standard ASTM C1793, "Guide to the Development of Specifications for Fiber Reinforced Silicon-Carbide Composites for Nuclear Applications," provides guidance for developing the detailed material specification for SiC/SiC composite core components. It lists test methods, which have either been developed or adopted for ceramic composites in nuclear applications as shown in Table 2.3. It also shows the outstanding test methods that need to be developed. Since its publication, ASTM C1819–15 has been published, which describes the test method for hoop strength properties.

Table 2.3. Test standards to be used for SiC/SiC composite materials. [25]

	Units	ASTM Test – Flats-Bars	ASTM Test – Rods/Tubes
Tensile Properties (ultimate, fracture, PropL)	MPa & strain	C1275, C1359	C1773
Flexure Properties (ultimate, fracture, PropL)	MPa & strain	C1341	[B]
Compression Properties (ultimate, fracture, PropL)	MPa & strain	C1358	[B]
Shear Properties (ultimate, fracture, PropL)	MPa & strain	C1292, C1425	[B]
Transthickness Tensile Properties (ultimate, fracture, PropL)	MPa & strain	C1468	[B]
Hoop Strength Properties (ultimate, fracture, PropL)	MPa & strain	NA	[B]
Elastic/Shear Modulus by Mechanical Loading	GPa	E111, E143	E111[A] , E143[A]
Elastic/Shear Modulus by Sonic Resonance	GPa	C1198	C1198[A]
Elastic/Shear Modulus by Impulse Excitation	GPa	C1259	C1259[A]
Elastic Modulus by Sonic Velocity	GPa	C769	C769[A]
Poisson's Ratio	nd	E132	E132
Modulus of Resilience (in Tension)	J/m^3	C1275, C1359	C1773
Modulus of Toughness (in Tension)	J/m^3	C1275, C1359	C1773
Open Hole Tensile Strength Properties	MPa & strain	D5766[A]	[B]
Open Hole Compression Strength Properties	MPa & strain	D6484[A]	[B]
Notch Tensile Strength Properties	MPa & strain	[B]	[B]
Notch Compression Strength Properties	MPa & strain	[B]	[B]
Pin Bearing Strength Properties	MPa & strain	D5961[A]	[B]
Crack Growth Resistance/ Strain Energy Release Rate/ (Fracture Toughness) (Interlaminar and Translaminar)	kJ/m^2	D5528[A] , D6671[A] , E1922[A]	[B]

[A] Modification of this polymer matrix composite test method may be required.
[B] New test methods are required.
nd = no dimensions.

For the structural design of composite core components, the ASME code provides for design-by-analysis and design-by-test. The design-by-analysis approach is available but is complicated by the lack of specific guidance, and the designers will have to develop and validate their own methods.

For the integrated structure, the distortion or deformation (due to temperature or irradiation) of individual composite core components should not cause constraints by hindering expansion or shrinkage. Furthermore, the differential strains inside the core assembly and in the surrounding structures should not lead to stresses that exceed the requirements for acceptability defined in the developed design rules.

The design rules do not make use of a theory for combining stresses. Instead, the design approach requires a comparison between the maximum stress (in the dominant failure mode) resulting from the loading of the component, and the stress (in the same mode) at failure of the material. Stress analysis is to be performed on unirradiated, irradiated and oxidized (the effect of chemical attack) composite core components. For the non-irradiated core components, an elastic analysis need to be performed without accounting for irradiation damage with the exception of thermal conductivity that is used for thermal stress prediction. (Lastly mentioned is for cases where the dose exceeds 0.001 dpa.) For analysis on the irradiated composite core components, irradiation-induced property changes on the material and the development of stresses in the components shall be accounted for. For analysis on oxidized core components, the effect of chemical attack on the dimensions and the distribution of material properties in the components shall be considered. The designer is responsible for the accuracy and acceptability of the analysis methods used. The allowable stress values depend on the POF, which is derived from the structural reliability class of the composite core component and the service level of the load. The design strength values for a defined POF are retrieved from the Material Data Sheet of the specific ceramic composite material. The allowable stress values for tensile stresses, compressive stresses, bending, and shear stresses are to be determined from the measured and defined material design strengths in tension, compression, bending, shear, or another failure mode, respectively.

It will be required to indicate the changes in physical and mechanical properties due to neutron irradiation and chemical interaction at sufficient intervals. Changes must be reported over the design fluence or chemical partial pressure and temperature ranges, as a function of fluence or as a function of the chemical partial pressure, in the case of irradiation and chemical attack, respectively. If the composite material is anisotropic, differentiation with respect to anisotropic orientation is required in reporting the property changes. An important takeaway is that SiC/SiC composites are used as a material by design instead of a material in design. The material architecture, and thus its properties, can be adjusted to match the application.

In completing the code design of the components, the general approach is to differentiate between primary loads (due to external forces or pressure) and secondary loads (due to irradiation induced swelling/shrinkage and incompatible thermal strains). This approach is generally applicable to MSRs as well.

For structural design, the experience, data, and/or models from HTGRs can be applied to FHRs [26] with a major operational difference that the primary loads tend to be lower for FHRs after reactor startup. Near-neutral buoyancy reduces the gravity loads, and pressures are near atmospheric. Considering the core structure, the graphite blocks will float in the salt if unrestrained. In general, the buoyancy effect will transfer the loads from the core barrel support plate to the upper core internals in the area where the control rod guide tubes are connected. The graphite structure will need to be tied down by upper and lower plates with weights higher than the buoyancy force. Reflector blocks may need to be kept circumferentially aligned by mechanisms like pins, keys, and/or belts that allow for radial thermal expansion.

The ASME composite code in its current state can be used as a base for FHRs. The FHR loads are expected to be different from HTGR loads, but itmust be considered to show that the structures maintain adequate levels of integrity throughout the design life. Furthermore, effects like thermal striping and flow-induced vibration are likely to be important in FHR designs while less significant to HTGR designs (because the salt is a better heat transfer material and more dense than helium). The code in its final stages would need to be reviewed to ensure that it makes sufficient provision to address these effects.

Additionally, the code may have to be assessed for its compatibility with LFMSR designs, with a focus on possible materials interactions with the actinides and fission products to be found in the coolant solution. In its current form, the code addresses how to design for chemical attack by radionuclides. Specific guidance may improve how the code addresses the effects caused by actinide and fission product interaction.

2.5 LICENSING ASPECTS

Aside from the ARE and MSRE test reactors, no MSR, specifically no FHR class reactor, has ever been constructed to serve as the basis for the safety, sustainability, or licensing case for U.S. Nuclear Regulatory Commission (NRC) review. However, the NRC has experience in previously licensed liquid metal reactors and HTGRs. Because the FHR combines existing MSR technology with proven high-temperature TRISO fuel technology like the HTGR, it supports a reasonably strong case for FHR licensing activities. The code in its current state under Section III subsection HH subpart B has matured to a point that it is close to publication and is applicable to HTGRs and solid fuel MSRs. Because of the lack of a demonstration reactor and a need to validate the rules, it is necessary to develop a technical basis document that supports the conditions described in the code with benchmarking data.

The licensing framework for solid fuel MSR design and analysis of passive safety and accident-ready systems, structures, and components is driven by earlier work done in the Next Generation Nuclear Plants (NGNP) forum and Pebble Bed Modular Reactor (PBMR) programs as discussed at various collaborative FHR workshops in the past few years [27-29]. The framework is mostly applicable to fuel but is possibly relevant to the safety design criteria for SiC components; which, in some instances, are part of the fuel assembly. The criteria include (1) maintaining core and reactor vessel geometry, (2) controlling heat generation (reactivity), and (3) maintaining control of radionuclides. Guidance from NUREG 1537 and NUREG 800 will likely be used as input for licensing of non-power test reactors and commercial reactors, respectively, after a gap analysis has been performed [13]. Another initiative under the DOE–Nuclear Energy Initiative–NRC licensing modernization program, the Licensing Technical Requirements Modernization Project, has the task of identifying gaps in the regulatory process for non-LWR designs, which includes HTRs and is performance based. It is possible that risk-informed licensing will form the basis for MSR regulation [30,31].

Without an operational reactor, the safety basis will rely on analyses supported by tests that rely on past operating experience. The information used is generated within a quality assurance program, typically in accordance with 10 CFR 50, Appendix B. This program may be implemented according to ASME NQA-1, considering a graded approach of applicability and importance.

Based on previous detailed system design analysis, mechanisms that can change the core internals and reactor vessel geometry include fuel movement, thermal expansion during normal transients, slow materials processes such as irradiation-induced swelling and corrosion, and thermal and mechanical stresses during transients and accidents. For the reactivity control systems, functional requirements applicable to the control rod sleeves may include ensuring the channel geometry for high-reliability insertion. This may be different in the case of liquid fuel designs, which have reduced safety performance requirements. Daily fuel addition and strong inherent negative temperature reactivity feedback results in minimal excess reactivity. The design rules discussed in the code largely address these mechanistic behaviors; but they do not include the use of ceramics as coating or barrier materials to act as a control for radionuclides, even though they address aspects regarding chemical attack. This is considered outside the scope of the code, which is to address and ensure pressure retention and structural integrity.

To close the gap for licensing, a skilled workforce who understand the underlying complexities of SiC/SiC composite materials and who are knowledgeable regarding the design approach are needed within the NRC and the wider community to overcome the remaining safety concerns.

As previously mentioned, the code may have to accommodate additional guidance associated with LFMSR designs detailing the effects of fuel interaction, which currently are not explicitly addressed.

2.6 THE TECHNOLOGY GAPS IN THE DESIGN METHODOLOGY

To enable the development and demonstration of an operating FHR for commercial deployment, several infrastructure and maturation goals have been identified [19]. They include developing and demonstrating a licensing path for advanced reactors in general, demonstrating key fabrication techniques for reactor components, and developing a supply chain for FHR-specific components and materials. Key system and component technologies include fuel assembly and control rod systems. SiC/SiC composites have been identified as a potential candidate for various components within these systems.

A number of activities have been undertaken, including establishing design rules and standards and generating experimental data on irradiation effects. Some of these activities are also supported by efforts from the LWR and advanced fuels technology communities that are driving the development of the SiC fuel cladding and core component applications for accident-tolerant fuel designs.

Significant progress has been made with regards to understanding the irradiation performance characteristics, but work is required to understand the mechanical design limitations for SiC/SiC composites. The stress applications for MSR designs are still unknown, and benchmark data validating the analysis of the structural design are required to support the limiting conditions described in the composites code. These needs can be supported by the development of a technical basis document. The code also needs to be assessed to ensure that it sufficiently addresses material effects due to material interactions with actinides and fission products.

For the development of the SiC/SiC composite Material Data Sheet/s, and in light of Table 2.3 as listed in ASTM C1793, there are still a large number of outstanding ASTM test standards that may be critical for composite core components—such as fuel or control rod sleeve applications. Some rod/tube test standards are in development, including

- Open-hole tensile strength of fiber-reinforced advanced ceramic composites
- Flexure tube strength at room-temperature testing

Other new standards, including “Guide to Oxidation Exposure Testing of Advanced Ceramics” and “Torsional Shear Strength of Advanced Ceramic Bonded Joints” are also in development.

Besides the current efforts, there are several rod/tube standards applicable to HTRs in general, such as compression, shear, trans-thickness tensile, and hoop strength properties (at room- and/or high-temperature testing). Pin bearing strength and crack growth resistance or strain energy release rate are listed as required test methods and need development. For molten salt applications, new test standards for high-temperature testing retained strength, degradation, and elastic constants in corrosive environments are important and currently lacking. A few existing test standards were identified that require modifications to incorporate SiC/SiC matrix composites. These tests include elastic/shear modulus by mechanical loading, sonic resonance, impulse excitation, and sonic velocity, as well as Poisson’s ratio, modulus of resilience, and modulus of toughness.

Once developed, the new standard tests need to be performed via interlaboratory round-robin testing, with the intent to conduct tests repeatedly under the same conditions and by doing so establish precision and bias statements to be adopted within the standards.

3. MATERIALS AND MANUFACTURING

3.1 COMPOSITES: FIBERS, MATRICES, AND INTERFACE

SiC materials of interest for nuclear structural applications are mostly continuous fiber-reinforced ceramics matrix composites, which consist of SiC fiber, SiC matrix, and a carbon interface between the fiber and matrix [32] (Figure 3.1). This section describes fabrication and integration technologies for potential MSR applications.

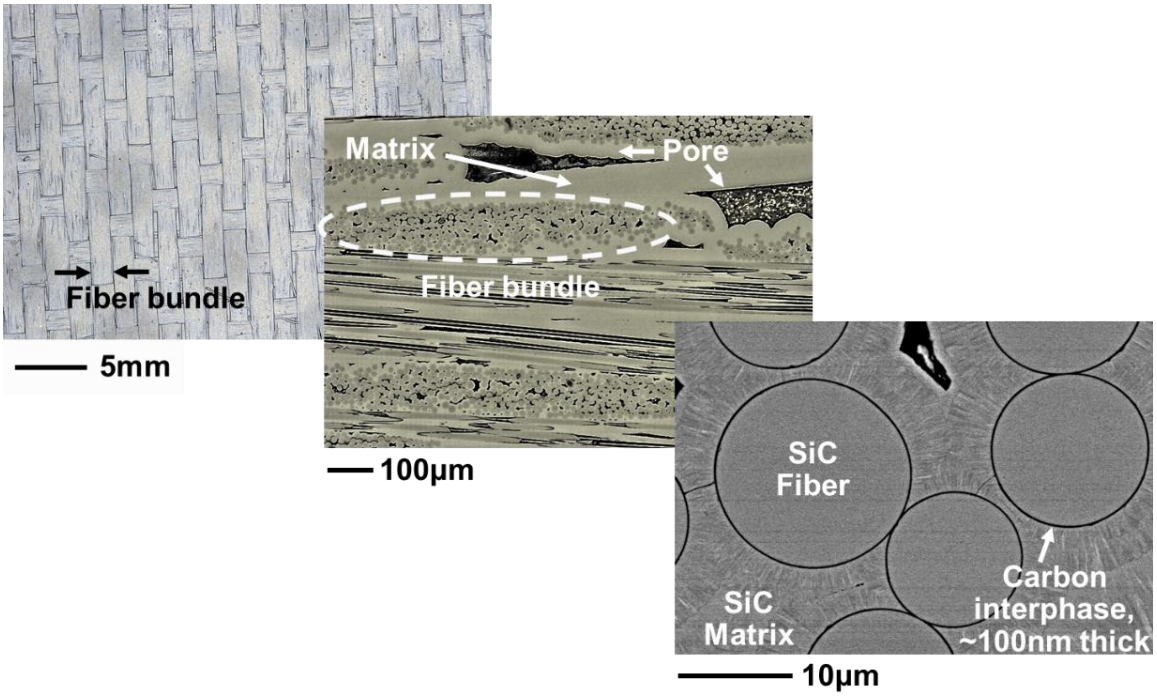

Figure 3.1. Appearance of continuous SiC fiber–reinforced SiC matrix composites fabricated by CVI.

3.1.1 Fiber

Fiber is a key element of SiC/SiC composites that determines the ultimate strength of a composite material [33]. Nuclear-grade SiC fiber is considered near-stoichiometric and highly crystalline because of its dimensional stability under irradiation compared with non-stoichiometric and amorphous-like SiC fibers [32]. This generation III class of SiC fibers that can be considered for nuclear applications includes Hi-Nicalon Type S (HNS; Nippon Carbon Co., Tokyo, Japan), Tyranno SA3 (SA3; Ube Industries Ltd., Ube, Japan), and Sylramic (SYL; COI Ceramics, San Diego). Information on the properties of these fibers can be found elsewhere [34]. Briefly, they have similar mechanical properties—Young's modulus of ~400 GPa and room-temperature tensile strength of >2 GPa—but their thermal properties may differ significantly. Only the HNS and SA3 SiC fibers are currently considered for nuclear applications because the boron (a neutron absorber) present in SYL is considered an impurity and makes it unfavorable.

Given certain properties for the constituent materials, the composite properties are determined by the fiber architecture. The reinforcing fibers provide benefits such as strength and toughness most effectively in directions parallel to the fiber axis. More precisely, the composite properties are to a large extent determined by the volume fractions and orientations of the fibers in relation to the orientation of interest for certain properties. Therefore, tailoring the fiber architecture is a key to optimizing the composite mechanical

properties [32]. In addition, fiber woven technology is essential for near-net shape processing. Currently, fiber architectures include 2-direction layups in the form of woven fabrics, 2.5-direction layups with cross weaving through the woven fabrics, and 3-direction orthogonal weaves. The architecture will be chosen depending on the property requirements. Examples of the fiber architectures with tube geometries are shown in Figure 3.2.

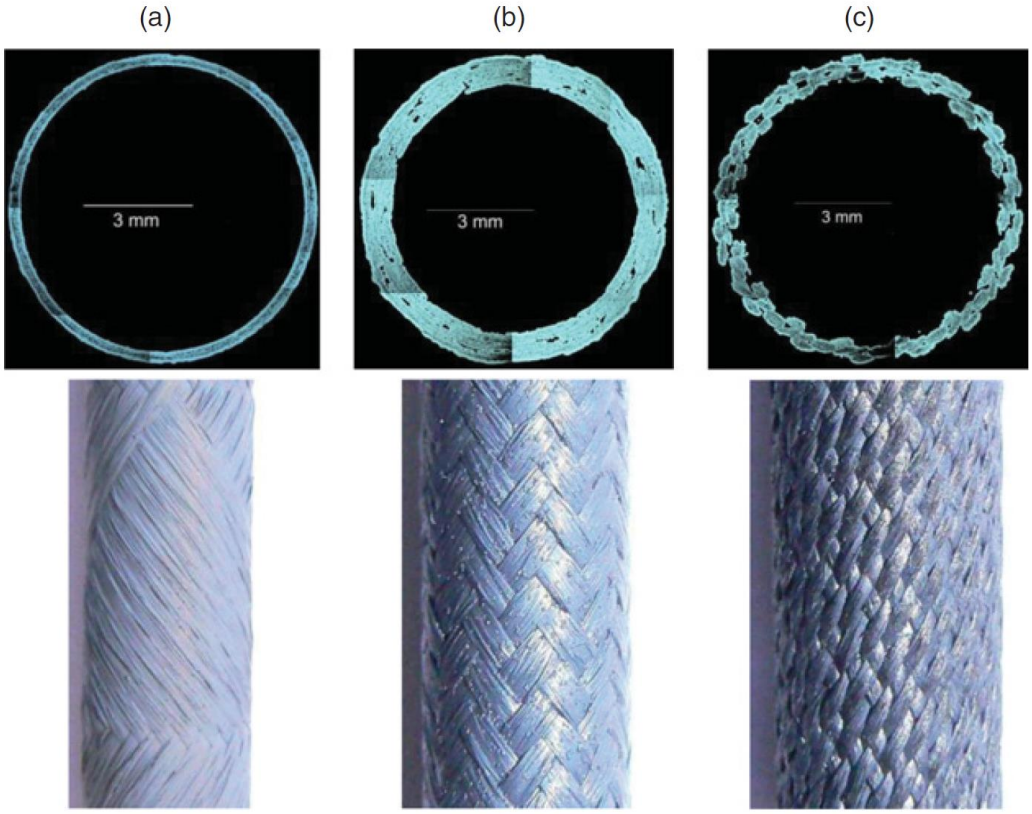

Figure 3.2. Examples of the fiber architecture of a CVI SiC/SiC tube: (a) filament winding, (b) 2-direction braiding, and (c) 3-direction braiding. Reprinted from [35].

3.1.2 Matrix

A matrix surrounds the carbon-coated SiC fibers. SiC/SiC composites are usually designed to have the matrix exposed to the reactor environment so that the matrix can protect the fiber and carbon interface. In addition, mechanical properties of the matrix are key factors that determine the crack initiation stress of the composites [36]. SiC/SiC composite densification routes that have been proved to produce radiation-resistant forms of composite materials are CVI (chemical vapor infiltration) [37] and SiC powder sintering represented by the NITE (nano-infiltration and transient eutectic phase) process [38]. These fabrication methodologies and the properties of the two types of matrixes are discussed below.

3.1.2.1 Chemical vapor infiltration matrix

CVI is currently the most reliable method of producing a matrix composed of the very high-purity, crystalline SiC that is necessary to provide good irradiation resistance for nuclear applications [32]. In addition, the CVI process is a relatively mature processing technology for fabricating SiC/SiC composites and is available in industries worldwide. In the CVI process, the deposition rate is one of the key processing parameters. High deposition rates during composite fabrication lead to high levels of internal porosity. Low

deposition rates are required to achieve low internal porosity, but they result in long fabrication times. Increasing the internal density of the matrix leads to improved mechanical and thermal properties [39]. Because of its high purity, a CVI SiC matrix makes the best use of the intrinsic potential of SiC, such as high-temperature capability, chemical stability, and irradiation resistance.

3.1.2.2 Nano-infiltration and transient eutectic phase matrix

The NITE process has demonstrated an almost fully dense SiC/SiC composite [38]. This achievement is beneficial to the fabrication of gas tight components without any additional processing such as a CVD SiC coating. NITE is a specific type of liquid-phase sintering for SiC/SiC composites: sintering of SiC fiber forms infiltrated with an SiC slurry consisting of an SiC powder with nano-size particles and oxide additives such as a eutectic composition of alumina and yttria [38]. NITE SiC/SiC tubes may be produced by a hot isostatic press, using a furnace of adequate size. Since the NITE matrix contains secondary phases attributed to the oxide additives, a key challenge for the MSR application is achieving a matrix resistant to reactor environments, including salt corrosion for normal operation.

3.1.3 Interface

The interface between the fiber and matrix significantly determines the fracture behavior of SiC/SiC composites. The advantages of SiC/SiC composites, including high toughness and reliable mechanical properties, are enabled by their fiber-matrix interface with adequate bonding strength and interfacial sliding strength. The primary tough fracture behavior of the ceramic composite is realized through the deflection of matrix cracks at the fiber/matrix interface without the breakage of fibers followed by fiber pull-out that is associated with frictional dissipation. Carbon-based interfaces, such as the monolayer pyrolytic carbon (PyC) interface and the multi-layer PyC/SiC interface (Figure 3.3) are proven to be irradiation resistant [32]. The interface is typically formed via a CVD process. The interface thickness has been reported to slightly affect mechanical properties such as ultimate tensile strength (UTS), proportional limit stress (PLS), Young's modulus, and strain to failure when plate specimens were tested [40].

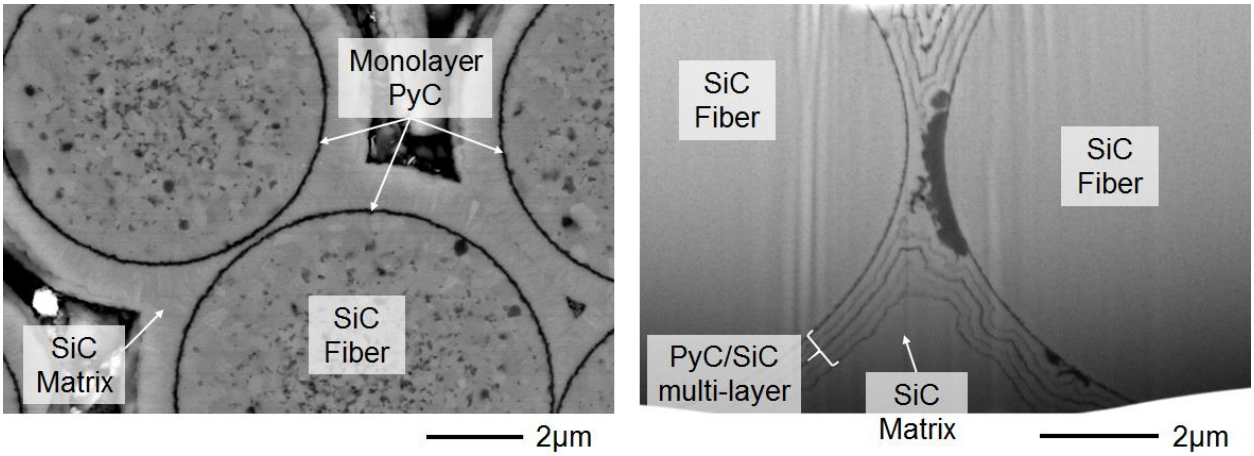

Figure 3.3. SEM micrographs of monolayer carbon interphase (left image) and carbon/SiC multilayer interphase (right image).

3.2 JOINING AND INTEGRATION TECHNOLOGIES

Joining technology enables the fabrication of a larger and/or complex-shape component. The joining and integration of SiC materials to other SiC materials are feasible and established technologies. The following sections explain (1) joint processing, (2) assembly technologies, and (3) properties of the joints.

3.2.1 Joint Processing

There are various options for joining SiC to SiC. The joining temperature should be low enough to avoid impacting the composite properties by annealing. The strengths of HNS and SA3 SiC fibers are known to degrade under annealing at ~1800 and ~1900 °C, respectively [41]. In the case of direct joining of SiC to SiC without any interlayer, solid state diffusion bonding of SiC can be produced under high temperature (>~2000°C) and high applied stress (>~15 MPa) [42]. Because the dual processing requirements of high temperature and pressure limit practical applications for SiC–SiC joining, SiC joining with an interlayer is frequently used. Several types of interlayer materials are available depending on the joining method. Solid state diffusion bonding typically uses refractory metals such as Ti, Mo, and W [43,44]. The processing conditions of metal diffusion bonding of SiC include temperatures below the 1200–1500°C range and applied stresses of ~10 MPa. Glass forming ceramics and metallic brazing materials are also available for SiC-to-SiC joining. These types of joining have been demonstrated at relatively low procession temperatures of <1500 °C and under low or no process applied stress [45,46]. Sintering SiC powder and processing additives, typically oxides, is another method of producing an SiC joint. Although relatively high processing temperatures (~1850°C) and high pressures (~20MPa) are required [47], this method forms an SiC-based bonding layer, which is expected to have similar properties to substrate materials. Selected-area CVD or CVI of SiC also provides an SiC bonding layer [48]. This process requires only limited applied stress during joining, although there may be limitations of the joining thickness. A detailed summary of SiC joining technology can be found in [47].

Fabrication technology is also available for joining SiC to metals. SiC-to-aluminum and SiC-to-steel joining have been demonstrated [49], although the demonstration of joining SiC to dissimilar materials (such as metals) was little reported because of the difficulty of doing so. Common hurdles to joining include the reactions between substrates and the residual stresses attributed to differential thermal expansion during joining at elevated temperatures. Therefore, further development of the joining technology is required in case joining SiC to dissimilar materials is desirable for MSR applications.

3.2.2 Assembly Technologies

In addition to joining, assembly technologies, which do not exhibit chemical reactions between components, are available for SiC/SiC composites. One example is mechanical joining, which has been demonstrated using screw-threaded tubes for machinable NITE SiC/SiC composite (Figure 3.4) [50]. NITE SiC/SiC composite was machinable because the material was dense and robust. Screw-thread joining is usually difficult for CVI SiC/SiC composite with typical ~10% porosity because of cracking during machining. The manufacture of a joint segment made of a CVI SiC/SiC composite has been demonstrated for a nuclear reactor control rod sheath [51]. Near-net-shape processing of CVI SiC/SiC composite components was conducted before the assembly of the control rod sheath, as shown in Figure 3.5(a). Near-net shaping is a key technology for fabrication of SiC/SiC components because of the difficulty of machining hard SiC ceramics. The assembled control rod sheath is shown in Figure 3.5(b). Assembly technology is available for both CVI and NITE SiC/SiC composites and enables the fabrication of complex components made only of SiC materials.

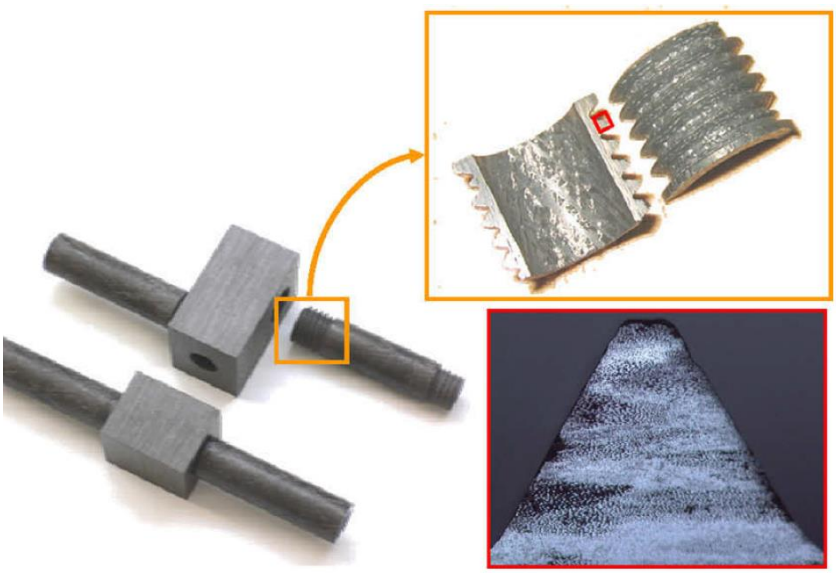

Figure 3.4. Screw-threaded NITE-SiC/SiC composite joint. Images reprinted from [50].

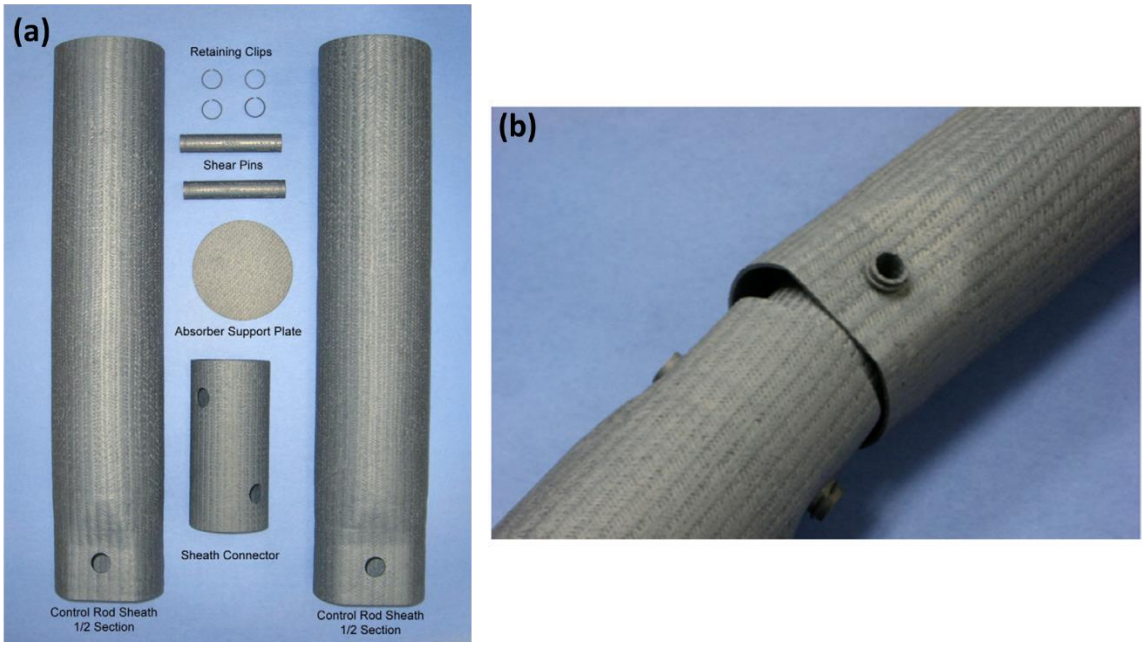

Figure 3.5. (a) CVI SiC/SiC control rod sheath components before assembly and (b) assembled CVI SiC/SiC control rod sheath joint segment. Images reprinted from [51].

3.2.3 Properties of the Joints

The selection of the type of joint for an MSR application should be based on not only processing capability but also the properties of the joints. Properties of interest include bonding strength, environmental resistance, and hermeticity. There are several methods available to evaluate joint strength. The shear strength of ceramics joints has been investigated using single-lap and double-lap offset tests, double-notch compression tests, asymmetrical four-point bending tests, and torsion tests [47,52]. Commonly, a weak joint exhibits failure at the bonding layer or joint/substrate interface. In contrast, a robust joint fails at, or

partially at, the substrate [47]. Most of the SiC-to-SiC joints described in Section 3.2.1. exhibited failure at the substrate or a mixture of failures at the substrate and bonding layer [43,46,47]. Therefore, robust SiC-to-SiC joints are available for various interphases. Environmental resistance is also important to selecting a joining method. Neutron irradiation at elevated temperatures and corrosive environments are expected for MSR applications. Effects of neutron irradiation on the strength of SiC-to-SiC joints with various interphases have been investigated [46-58, 53]. The irradiation temperature and neutron doses were 300–800°C and a few to 9 dpa, respectively. In short, all the joints tested retained a certain level of joint strength and an apparent torsional shear strength of ~100 MPa following neutron irradiation. However, irradiation-induced cracking was found in joints with non-SiC bonding layers, likely because of differential radiation-induced swelling between the SiC substrate and the bonding phases. SiC-based bonding did not show any indication of degradation by irradiation.

Salt corrosion resistance will be required for SiC joints; the knowledge gap remains the joint exposure to the salt. The hermeticity of the joint may also be an important consideration for selecting a joining method, depending on the functionality of the SiC component, although this property is rarely evaluated. The CVD/CVI SiC–based joint layer has been demonstrated to provide sufficient gastightness for LWR cladding applications [54]. It is expected that radiation-induced cracking of the non-SiC bonding layer will be an issue in the hermeticity of the joint, but the SiC-based bonding layers are not affected or limited.

3.3 FABRICATION OF SiC COMPONENTS

Fabrication technology is obviously necessary for MSR applications. Plate materials are usually fabricated and tested for evaluation of the properties of CVI and NITE SiC/SiC composites. However, a simple plate may not be useful for practical applications. This section explores current technologies for fabricating SiC components with different geometries and sizes. A long, thin wall tube made of SiC/SiC composites is a common interest for fuel claddings of fission reactors and SiC tube components may also be useful for MSR applications. Recently, General Atomics developed the capability to produce ~1 m long tubes via a CVI process with adequate straightness, wall thickness uniformity, roundness, and reproducibility of surface roughness [54] (Figure 3.6). This fabrication technology is being advanced to produce full-length (~4 m) fuel cladding. SiC/SiC composites are also of interest for the channel boxes of boiling water reactors. A section of a thin-wall channel box made of CVI SiC/SiC composite has been fabricated and evaluated [55]. The appearance of the channel box can be seen in Figure 3.7. The CVI process is applicable for the fabrication of a thin structure, as demonstrated by the fabrication of the tube and the channel box. In addition, a near-net-shape CVI process is feasible because the CVI process involves the infiltration of SiC forming chemicals into a pre-formed fiber structure. On the other hand, it may be difficult to fabricate a thick component using CVI. CVI is a scalable technology that requires a large CVI furnace for the fabrication of large and/or long components.

NITE process also enables production of components with different shapes, including thick blocks, combustor liners, thin plates, and tubes, as shown in Figure 3.8 [56]. Such large or complex-shape components can be fabricated via hot pressing or hot isostatic pressing. NITE is also a scalable method for fabricating large components using a large sintering furnace.

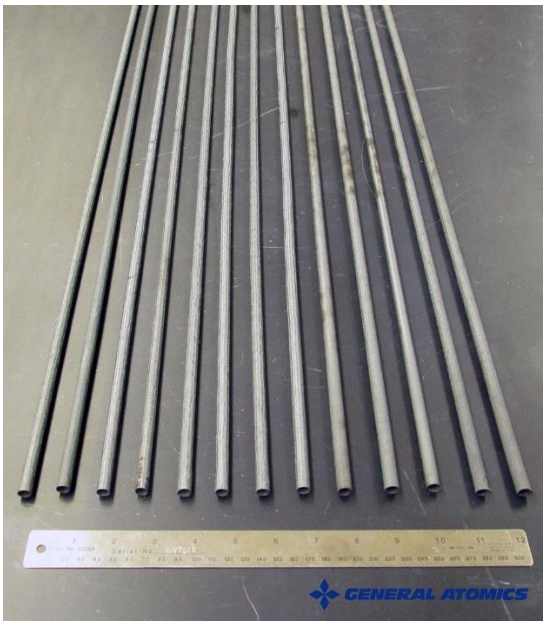

Figure 3.6. Long SiC/SiC composite tubes fabricated by CVI process. [54]

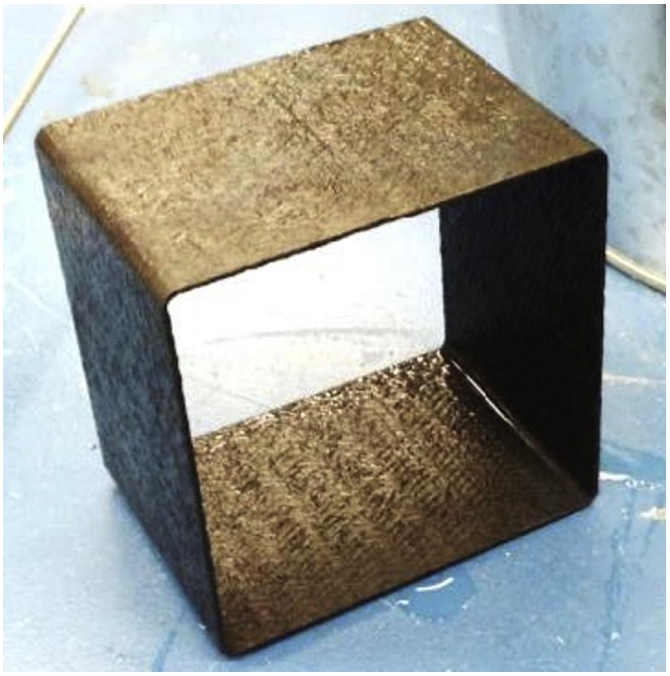

Figure 3.7. Section of channel box made of CVI SiC/SiC composite. [55]. The channel box is 7.6 cm in height.

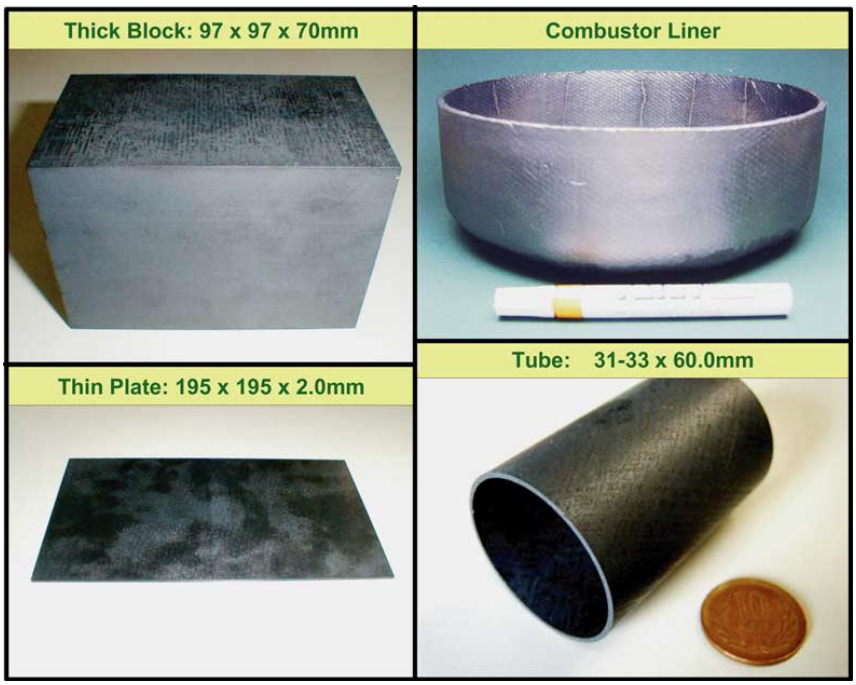

Figure 3.8. NITE SiC/SiC composites in various product forms. [56]

Various components made of fiber-reinforced ceramic composites have been fabricated for aerospace applications. The benefits of using SiC/SiC composites rather than high-temperature alloys are improvement of energy efficiency due to weight reduction and ability to withstand higher operational temperatures. Although the material is usually a non-nuclear-grade SiC/SiC composite or non-SiC composite, the fabrication technology can be applied for the fabrication of nuclear-grade SiC/SiC composite components. The common processing technology, regardless of material type, includes fiber weave processing to form large and/or complex-shape geometries. Once a fiber preform is prepared, it is possible to produce a SiC matrix via CVI or NITE. Figure 3.9 shows a SiC/SiC composite turbine vane [57]. This complex component was fabricated without introducing significant damage in the fiber during processing. One of the largest components made of a ceramic composite is a C/SiC body flap for flight control during the re-entry of a space vehicle (Figure 3.10) [58]. The material was fabricated using polymer and CVI processes. The component was about 1.5 m in length. Mechanical joining was used to assemble the different C/SiC parts. This example shows the possibility of fabricating a large component made of nuclear-grade CVI SiC/SiC composites because of the similarity of the fiber weaving and matrix densification processes.

In addition to fabrication, there are other common development interests among nuclear and aerospace applications, including thermo-mechanical modeling capabilities, nondestructive evaluation methods, optimization of fiber architectures, assessment of material life, material designs and codes, and several other areas. Moreover, current experience in the use of SiC/SiC composites in jet engines is expected to advance the use of SiC/SiC composites as structural components of nuclear reactors. This is of critical importance because SiC/SiC composites have much less structural application experience and fewer data compared with metals. Aerospace development is expected to provide a significant benefit for nuclear material engineering development.

Figure 3.9. SiC/SiC composite turbine vane fabricated by the National Aeronautics and Space Administration. [57]

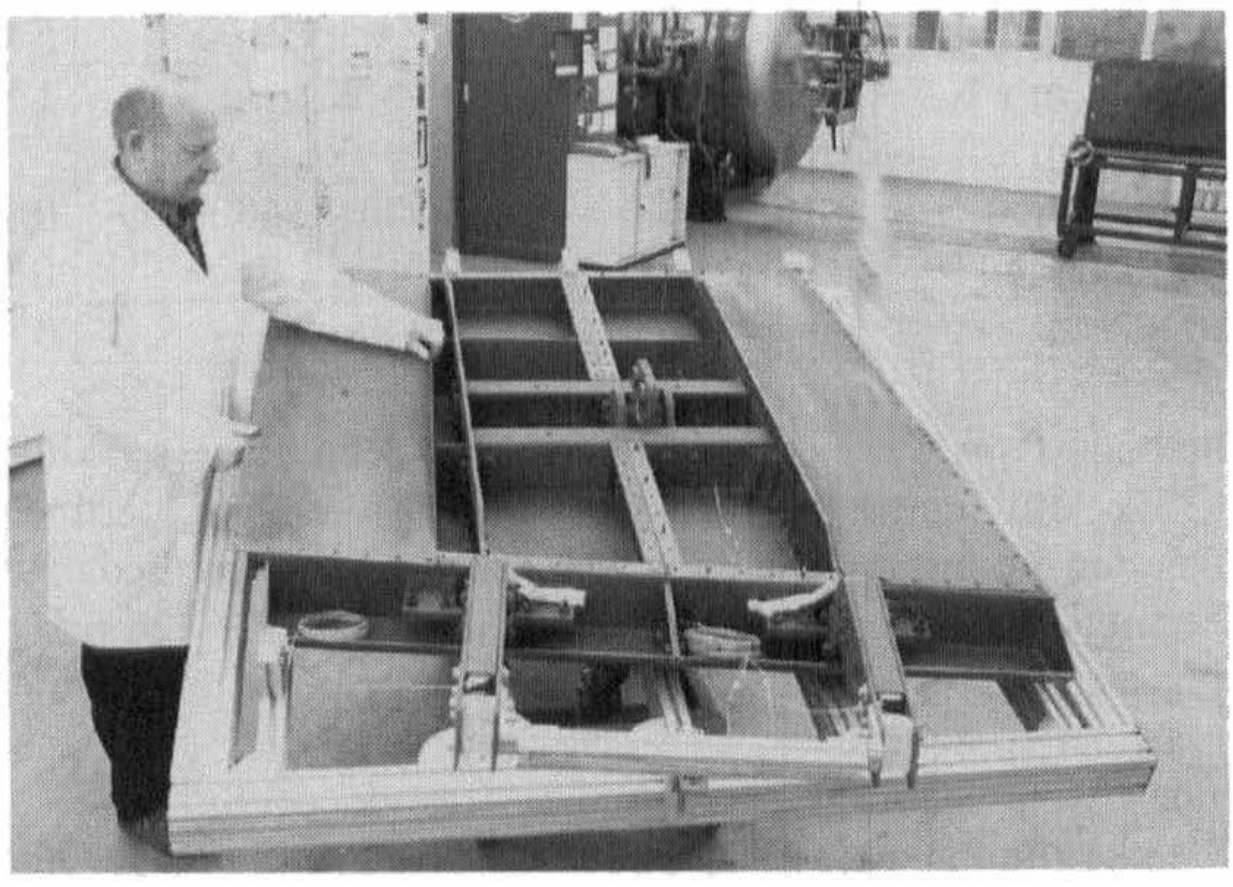

Figure 3.10. Appearance of body flap made of polymer/CVI C/SiC composites. [58]. The length was about 1.5 m.

3.4 TECHNOLOGY GAPS FOR SiC/SiC MATERIALS AND MANUFACTURING

For viable use of nuclear-grade SiC/SiC composites in MSR applications, it will be necessary to fabricate large and/or complex-shape components. Although processing elements such as the fiber weaving process, matrix densification, and joining/integration technologies are available for SiC/SiC composite materials, demonstrations of component fabrication will be required. As mentioned in Section 2.4, design of the SiC/SiC component is also required. Since the thermo-mechanical properties of SiC/SiC composites are anisotropic and are tailorable, the fiber architecture and volume and the materials used in composite constituents need to be optimized. Selection of the integration method will be key, as the limitations for the joining process include minimizing processing damage to the composite. Furthermore, joints will need to withstand typical reactor environments.

4. PROPERTIES AND RADIATION EFFECTS

4.1 IRRADIATION EFFECTS

Research and development of SiC ceramics and composites for various applications under different reactor operating conditions has accumulated irradiation data for various temperature and dose conditions. Currently, a rich database of mechanical and physical properties of irradiated monolithic SiC [59] and SiC/SiC composites [32] are available. Such data are essential to assess the in-pile thermo-mechanical performance of SiC-based components. This section presents key properties of SiC materials for nuclear structural applications and identifies knowledge gaps in understanding the thermo-mechanical performance of SiC materials in MSRs. In this section, 1 dpa-SiC is assumed to be equivalent to a dose of 1×10^{25} n/m^2 (>0.1 MeV) [60].

4.1.1 Dimensional Stability

Dimensional stability under irradiation is mainly characterized by swelling and irradiation creep, which potentially determine the service life of reactor core components. Swelling of high-purity SiC and CVI SiC/SiC composites along the in-plane direction are very similar [61]. Swelling of SiC materials increases with increasing neutron dose up to ~1 dpa and then saturates at temperatures ranging from ~200 to ~1000°C [59]. Recently, this saturation swelling has been confirmed up to ~100 dpa [62]. The magnitude of swelling is inversely proportional to the irradiation temperature. The details of swelling behavior are shown in Figure 4.1. At irradiation temperatures above ~1000°C, the lifetime neutron dose of SiC is potentially determined by the requirement for dimensional stability, because SiC swelling is dose dependent [60].

Irradiation creep is a property that determines the dimensional stability under stress. Creep is known to be accelerated under irradiation environments because of the generation of irradiation-induced defects. In the case of SiC, irradiation creep has been explained by anisotropic swelling (more swelling along the tensile stress direction) up to high doses [63, 64]. Irradiation creep strain of SiC has been shown to be significantly smaller than the swelling; the instantaneous creep coefficient (stress-normalized creep strain) is 1×10^{-5} dpa^{-1}MPa^{-1} at 0.1dpa and 1×10^{-7} dpa^{-1}MPa^{-1} beyond 1dpa for most monolithic SiC forms and SiC fibers [63, 64]. Therefore, the dimensional stability of SiC in an irradiation environment is mainly characterized by swelling. Although there is currently little understanding regarding irradiation creep of SiC/SiC composites, the current data set suggests that it won't be a major issue for nuclear structural applications because of the small creep strain of composite constituents, including both matrix and fibers [64].

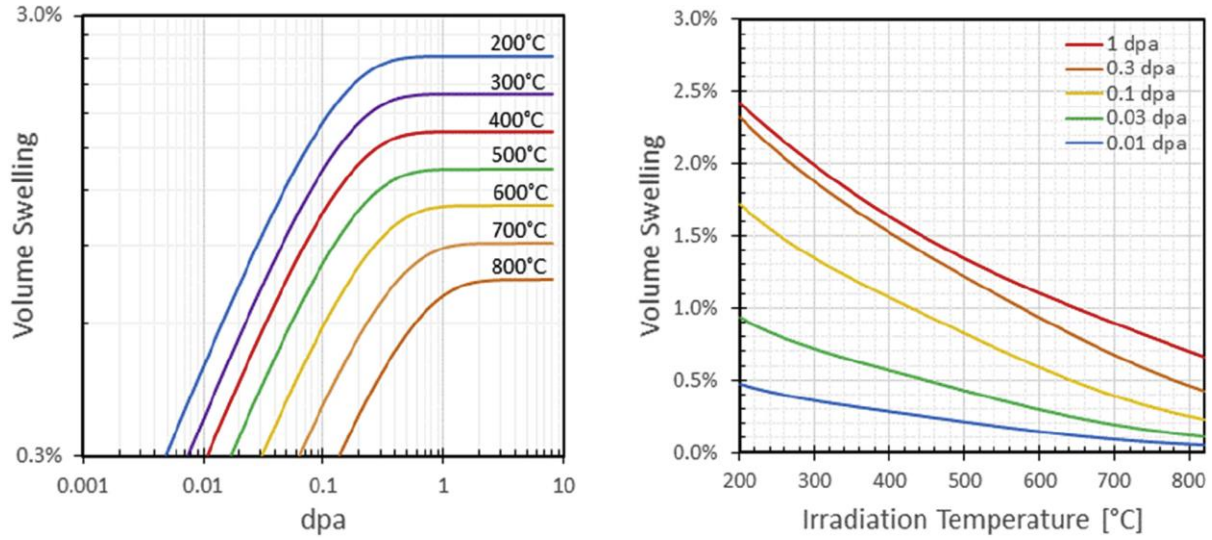

Figure 4.1. Neutron dose and temperature dependence of swelling of SiC. [61]

4.1.2 Mechanical Properties

SiC/SiC composites exhibit quasi-ductile fracture behavior, which is described by PLS and UTS in tension. Typical PLS and UTS have been reported to be ~100 and ~300 MPa, respectively, for nuclear-grade CVI SiC/SiC composites without irradiation [32]. Previous irradiation studies of SiC/SiC composites found insignificant degradation of the mechanical properties following irradiation at 300–1300°C to a low neutron dose (<~10 dpa) [32]. Effects of high-dose neutron irradiation of SiC/SiC composites were reported for only one specific type of material: a CVI SiC composite with Hi-Nicalon-TM Type S fiber coated with a PyC/SiC multi-layer interphase [62, 65]. These studies found irradiation temperature–dependent degradation of the material. The degradation of PLS and ultimate flexural strength (UFS) were limited or moderate following irradiation at 800°C up to 70 dpa. However, the strength degradation was more significant with decreasing radiation temperature, as shown in Figure 4.2a and b. Moreover, the composites showed brittle fracture following irradiation at 300°C to 92 dpa [62]. At temperatures below ~600°C, interphase and/or fiber degradation due to irradiation are associated with composite degradation, as found by microscopic investigation [62]. For the Young's modulus of composites, the degradation was limited to ~20% up to high doses (Figure 4.2 (c)). In short, the lifetimes of current nuclear-grade SiC/SiC composites are highly affected by the high-dose neutron irradiation at relatively low irradiation temperatures.

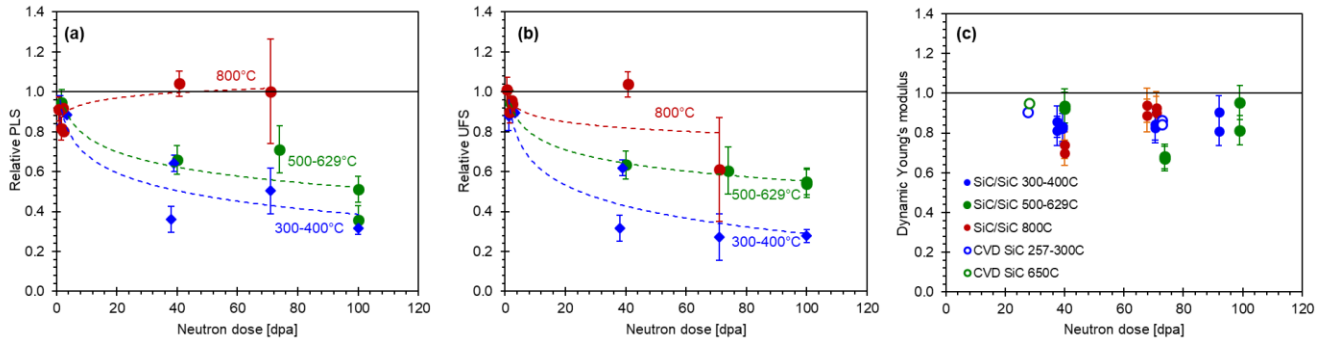

Figure 4.2. Neutron dose dependence of (a) PLS, (b) UFS, and (c) dynamic Young's modulus of CVI SiC/SiC composite with Hi-Nicalon Type S fiber coated with a PyC/SiC multi-layer interphase. [62]. The broken lines in (a) and (b) are fit by a logarithmic function to show the trend.

4.1.3 Thermal Properties

Thermal conductivity is another key physical property in assessing the performance of reactor materials. Thermal conductivity is defined by multiplying the density, specific heat capacity, and thermal diffusivity. The thermal conductivity of dense, high-purity, polycrystalline CVD SiC with a few micron grains is reported to be ~300 $Wm^{-1}K^{-1}$ at ambient temperature [59]. The room-temperature thermal conductivity of CVI SiC/SiC composites ranges from 8.5 to 53, mainly depending on the amount and distribution of the pores (typically ~10%) [32]. Therefore, the maximum thermal conductivity value of SiC components is the value of monolithic high-purity SiC (practically polycrystalline SiC). The thermal conductivity of SiC decreases with increasing temperature, and the value for that type of high-purity monolith has been reported to be ~140 $Wm^{-1}K^{-1}$ at 500°C and ~90 $Wm^{-1}K^{-1}$ at 1000°C [59].

The thermal conductivity of SiC is largely affected by the presence of irradiation-induced defects. Although the specific heat capacity and density of SiC are insignificantly modified by irradiation, its thermal diffusivity decreases significantly [59]. The room-temperature thermal diffusivity of high-purity CVD SiC has been investigated following irradiation at a wide range of temperature and dose conditions, as shown in Figure 4.3 [59]. The higher the irradiation temperature, the higher was the thermal conductivity, which is related to recovery of radiation defects at elevated temperatures. The thermal conductivity was ~13 $Wm^{-1}K^{-1}$ following neutron irradiation at ~500°C to 1–6 dpa. Neutron irradiation similarly decreases the thermal conductivity of CVI SiC/SiC composites; the value was a few $Wm^{-1}K^{-1}$ following neutron irradiation at ~500°C to 2.4 and 3.9 dpa [32]. Recent work found that the reduction of thermal diffusivity of CVI SiC/SiC composites saturated from ~1dpa to ~70 dpa at 300, 500, and 800°C [65]. The thermal conductivity of sintered SiC forms and NITE SiC/SiC composites are also reported [38, 66]. The thermal conductivities of these materials tend to be higher than that of CVI SiC/SiC composites but lower than that of high-purity dense SiC. Neutron irradiation significantly decreases the thermal conductivity of sintered SiC ceramics, similar to the case of CVD SiC and CVI SiC/SiC composites [66].

The coefficient of thermal expansion (CTE) is another important thermal property that defines the dimensional stability of materials at elevated temperatures. The CTE of nonirradiated β-SiC (α) in the temperature range 125–1273K has been reported as

$$\alpha = -1.8276 + 0.0178T - 1.5544 \times 10^{-5} T^2 + 4.5246 \times 10^{-9} T^3 \ (10^{-6}/K) , \quad (1)$$

where *T* is temperature [59]. A similar CTE was also reported for sintered SiC, which is relevant to the matrix of NITE SiC/SiC composites [67]. Importantly, there was no notable modification of the CTE of CVD SiC by neutron irradiation at 300, 500, and 800°C to ~70 dpa [65].

In summary, all nuclear-grade SiC materials exhibited irradiation-induced reduction of thermal conductivity, which may be a key factor in assessing the in-pile performance of SiC components in MSRs.

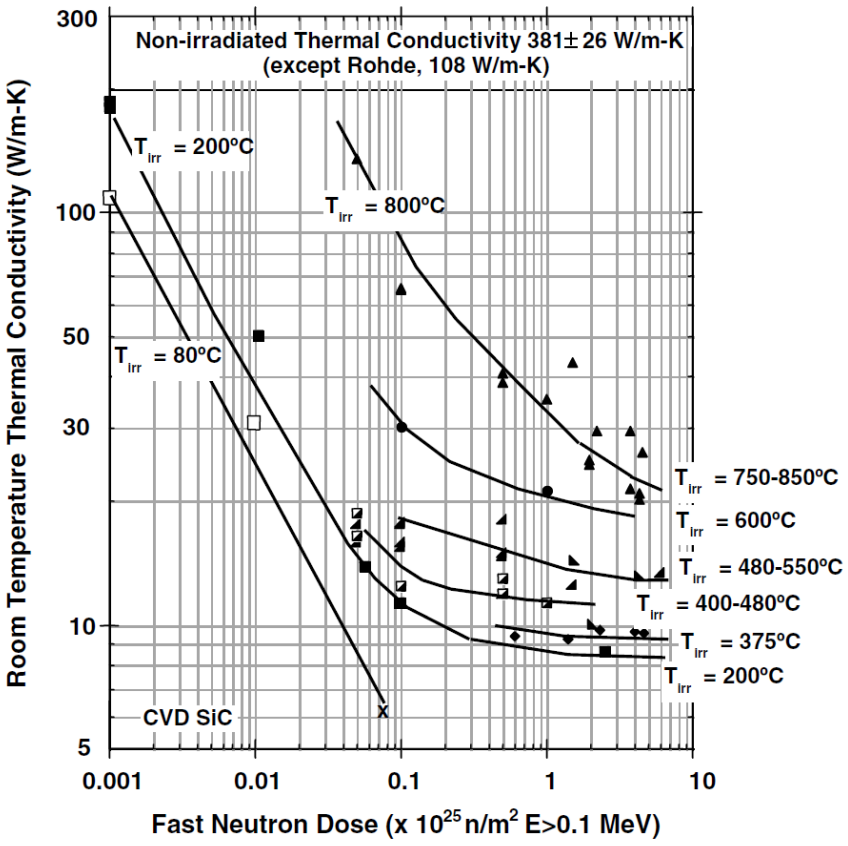

Figure 4.3. Room-temperature thermal diffusivity of neutron-irradiated CVD SiC. [59].

4.2 MICRO-CRACKING RELATED ISSUES

This section discusses how micro-cracks are formed in SiC/SiC composite materials and the effects of such cracks on the in-pile performance of SiC-based components. The fracture behavior of continuous-fiber SiC/SiC composites can be characterized by their PLS and UTS. The PLS is nearly equal to the stress level causing a critical matrix cracking event. However, micro-cracking has been detected at stress levels lower than the PLS [68]. Micro-cracks are found even in as-fabricated SiC/SiC composites without applied stress, as shown in Figure 4.4. The crack formation may be due to differential CTEs among the fibers, matrix, and interphase and to thermal stress caused by temperature gradients within the material during processing.

The micro-cracks themselves may not significantly degrade the mechanical properties of the composites [68]. However, time-dependent slow crack growth failure of nuclear-grade SiC/SiC composites has not been widely investigated. In MSR environments, surface cracks may cause salt ingress into materials, which may accelerate crack growth and salt corrosion. In this case, understanding corrosion-accelerating cracking and the corrosion resistance of composite constituents are important factors in assessing the salt ingress issue.

The issue of molten salt ingress has also been discussed for carbon materials [69]. Salt ingress is associated with the intrinsic corrosion resistance of the carbon material and porosity within the material. In the case of SiC/SiC composites, micro-cracking is one of the controlling mechanisms, as mentioned earlier, because the SiC component surface is expected to be a dense SiC in which the fiber and interphase are not exposed.

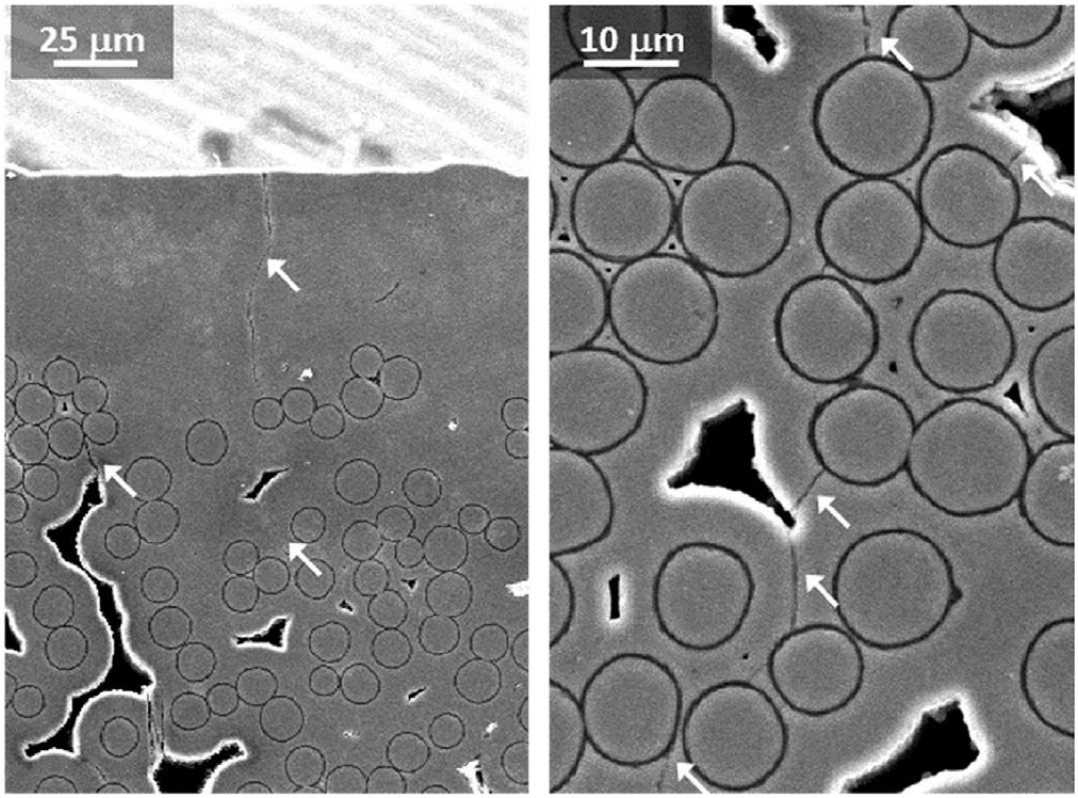

Figure 4.4. Micro-cracks found in as-fabricated CVI SiC/SiC composite. [61]

4.3 TECHNOLOGY GAPS IN THE PHYSICAL/MECHANICAL PROPERTIES AND RADIATION EFFECTS

SiC/SiC composites are now being developed as engineering materials for nuclear applications, since much early research in laboratory-grade materials has defined the material behavior and identified areas for improvement and in-depth evaluation. Therefore, key future research areas will be related to engineering issues. One of the technology gaps is assessment of material lifetime based on creep, fatigue, and corrosion. For MSR applications, slow crack growth under salt corrosion environments is a critical feasibility issue that has been insufficiently explored. For the issue of micro-cracking, statistical assessment of cracking probability, understanding of the nature of cracks under different loading and corrosion conditions, and establishment of test procedures to investigate slow crack growth are important areas of research. Comprehensive studies of microcracking issues should provide criteria for failure of SiC/SiC composites due to slow crack growth in MSRs.

In addition to those engineering issues, fundamental research is needed to address several issues. One of the major areas is a more complete understanding of irradiation effects. Material degradation due to high-dose neutron irradiation is a critical feasibility issue when the application temperature is relatively low and neutron dose is high. SiC/SiC composites resistant to high-dose irradiation will offer a competitive advantage if it is demonstrated that the core components can last substantially longer in their operating environments. As a result of the recent findings of degradation of PyC interphases and Hi-Nicalon Type S fibers at high doses [62, 65], it is necessary to optimize fiber/matrix interface design and materials for MSR applications. The synergy between neutron irradiation and environmental effects, including salt corrosion and applied stress/thermal stress, also needs be addressed.

5. CHEMICAL COMPATIBILITY

5.1 MODES OF SiC CORROSION

The corrosion of SiC in fluoride salts is a complex process. The surface corrosion behavior includes both electrochemical and non-electrical (e.g., chemisorption) interactions. Also, the potential permeation of tritium, in particular, affects the microstructure. In any MSR design, multiple materials will be in contact with the same flowing salt. It is important to recognize that, in a reactor, the SiC will not be exposed to pure salt, because any other material that is corroded in the system can travel through the salt to interact with the SiC. The instability of other structural materials, such as container alloys and graphite in molten fluoride salt, may accelerate SiC corrosion. The molecular dynamics and thermal hydraulics behavior of the salt further complicate the overall corrosion mechanism. Regions of hot and cold, flocculation, density distributions, thermal gradients, and flow conditions are probably best simulated in a flowing loop experiment.

The Chinese Academy of Sciences recently demonstrated some preliminary SiC corrosion experiments with container alloy constituents. These are static, sealed capsule tests with unirradiated SiC. In a glovebox, an argon cover gas is used to seal SiC in capsules made of graphite, SiC, or metal. Open capsule testing could be used for on-line corrosion potential measurements via electrochemical techniques. The following is a summary of the current results for SiC corrosion with container alloys. These preliminary studies have explored impurities-based corrosion in static corrosion tests, but thermal gradient–based corrosion experiments with loop testing have not yet been performed for SiC.

Knowledge of corrosion tendency (Gibbs free energy), corrosion rate kinetics, and solubility limit of SiC are significant technical gaps.

5.1.1.1 SiC corrosion capsule experiments

SiC may be exposed to dissolved metal ions from container alloys such as Cr^{2+}, Cr^{3+}, and Ni^{2+} from Hastelloy N. Hastelloy N is a nickel-based alloy considered for containers and salt-containing piping. Some recent preliminary data by ***Xue et al.*** show that Cr^{3+} from Hastelloy N aggravates the corrosion of SiC and forms chromium carbides as the main corrosion products [70]. Xue et al. tested CVD SiC samples in FLiNaK in sintered SiC capsules at 700°C for 15 days, then SiC with Hastelloy N, and finally SiC with CrF_3 to study Cr^{2+}[70]. For corrosion tests of CVD SiC in purified FLiNaK, cross-sectional line-scanning EDS (energy-dispersive x-ray spectroscopy) spectra showed that corrosion resulted in the loss of elemental silicon and the formation of a C- and O-rich surface. This result showed slight corrosion of CVD SiC in purified FLiNaK with a depth of 2.5 µm. For CVD SiC samples corroded in molten FLiNaK salt with CrF_3, cross-sectional scanning electron microscopy (SEM) showed that the corrosion depth was greater than 12.5 µm. Cross-sectional electron probe microanalysis (EPMA) showed that silicon content was lower near the surface corrosion than near uncorroded regions. Silica was initially detected with XPS in CVD SiC as-received from Dow Chemical. High-resolution x-ray photoelectron spectroscopy (XPS) analysis of Si^{2p} and O^{1s} peaks before and after corrosion in pure salt showed that the peak for Si-O, corresponding to SiO_2, and Si^{3+}-O peaks were not detected after corrosion, which could indicate that SiO_2 dissolved into the salt. The work of ***Zaykov et al.*** demonstrated the solubility of silica in a fluoride-chloride melt depending on the melt composition [71]. High-resolution XPS scans of O^{1s} peak before and after CrF_3-SiC corrosion also showed that peaks corresponding to Si-O disappeared after corrosion tests. High-resolution Cr^{2p} scans showed the corresponding Cr-O interactions and Cr-C bonds of Cr_7C_3 and Cr_3C_2. Grazing incidence x-ray diffraction (GI-XRD) results were consistent with the XPS results for chromium carbides and showed that the CrF_3 formed carbides, mainly Cr_7C_3 and Cr_3C_2, as corrosion products for the Cr^{3+} reaction with SiC. The CVD SiC samples corroded in FLiNaK with Hastelloy N showed that NiF_2 would form silicides.

Yang et al. studied the corrosion of SiC in FLiNaK at 700°C with added CrF_2 and NiF_2 in an SiC capsule for 15 days and 45 days, respectively. Yang et al. showed that when Hastelloy N is corroded by molten salt forming fluorides, such as NiF_2, the alloy and its corrosion products can aggravate SiC corrosion, which proceeds through silicide formation ($Ni_{31}Si_{12}$) [72]. They first looked at corrosion of SiC in pure FLiNaK. Raman spectroscopy before and after corrosion of CVD SiC in pure FLiNaK at 700°C in 15 days showed a disorder peak (D peak) and a graphitic peak (G peak) consistent with those of a graphite-rich layer. Then they looked at Hastelloy N samples and SiC in the same SiC capsule in FLiNaK. The cross-sectional EDS line-scan showed that Ni, Cr, Fe, and Mo diffuse outward to the alloy surface; but Fe and Mo accumulate near the surface, while Ni and Cr dissolve into the salt. Glow discharge mass spectroscopy (GD-MS) of FLiNaK after corrosion showed the silicon content in FLiNaK increased. To study Cr^{2+} effects on SiC corrosion, CrF_2 and SiC were immersed in FLiNaK in the same SiC capsule; for Ni^{2+} effects on SiC corrosion, SiC was immersed in FLiNaK mixed with NiF_2. The results showed that Cr^{3+} drives SiC corrosion by forming chromium carbides and a graphitic carbon layer. Hastelloy N experienced chromium corrosion, forming fluorides (Cr_xF_y) that aggravate SiC corrosion by driving silicon out of SiC into the melt, forming SiF62- [72]. Corroded regions were explored with XPS and GI-XRD patterns, which detected Cr_7C_3 and Cr_3C_2. For Ni^{2+} corrosion, GI-XRD patterns revealed that the CVD SiC surface coating composed of ß-SiC of about 50 µm disappeared after about 45 days, but the corrosion of simultaneously immersed Hastelloy N and SiC were not as severe.

Nishimura et al. studied SiC compatibility in FLiBe using a nickel crucible and found a thick silicide layer deposited on the surface of SiC. According to Nishimura et al., the silicide layer is $Ni_{31}Si_{12}$ that may be the product of Ni and Ni^{2+} reaction with SiC [73]. The effect of corrosion product Cr^{2+} was studied in the same way with SEM and GI-XRD. For the capsules with CrF_2, GI-XRD detected a new film of Cr_7C_3; and for capsules with Hastelloy N and SiC, GI-XRD showed the new film was Cr_7C_3, CrC, and Fe_4C. Silicon was detected in the salt with GD-MS, and the graphitic phases were attributed to the dissolution of silicon into the salt melt.

Some preliminary data from Yang et al. showed that when Hastelloy N (a nickel-based superalloy) is corroded by molten salt forming fluorides, such as NiF_2, the alloy and its corrosion products can aggravate SiC corrosion, which proceeds through silicide formation (Ni_xSi_y) [72]. Xue et al. showed that at 700°C for 400 hours, Hastelloy N experienced chromium corrosion, forming fluorides (Cr_xF_y) that aggravated SiC corrosion by driving silicon out of SiC into the melt, forming SiF_6^{2-} and different stoichiometries [70].

5.1.1.2 Pourbaix diagrams

A Pourbaix diagram shows the possible stable phases in an aqueous electrochemical system by plotting the potential for different redox states of an element as a function of pH, for instance. A Pourbaix diagram of the SiC, metal, graphite interactions in FLiBe and subsequently for FliNaK would be two important research milestones which have not been addressed. Corrosion potentials are redox potentials measured during corrosion that can be used to create Pourbaix diagrams. The diagram summarizes the conditions of redox potential and oxide concentration in which significant corrosion or precipitation can be avoided. Commonly used for metals, Pourbaix diagrams show three regions: regions where corrosion may or may not occur. Metals that are applied in structures and components are in the passive region.

Pourbaix diagrams are useful for predicting the spontaneous direction of electrochemical processes and corrosion products based on the potential and pH that result in a low or severe corrosion attack [74]. The example diagram, Figure 5.1, was constructed with the Gibbs free energy change, and the E-pH dependent reactions were calculated using the Nernst equation. The vertical lines are independent of potential but dependent on pH, with no electron transfer. The sloping lines give the redox potential of a solution in equilibrium with hydrogen or oxygen, respectively. This equilibrium indicates electron transfer as well as pH. The concentration of all metal ions is assumed to be 10^{-6} mol/L of solution, and at lower concentration,

corrosion should not occur. The diagram is computed for the equilibrium conditions at 25°C. The upper end of the redox potential axis is the noble end and the lower end is the active end, meaning that the oxidizing power increases with increasing potential. The water redox lines for hydrogen and oxygen are indicated in Pourbaix diagrams by dashed lines in the background, and water is stable only in the region between the dotted lines. For an element such as chromium, water redox lines have special significance. Lines indicate where two species exist in equilibrium, much like a standard phase diagram. Pure redox reactions are indicated by horizontal lines and are not pH dependent. Pure acid-base reactions are vertical lines and do not depend on potential.

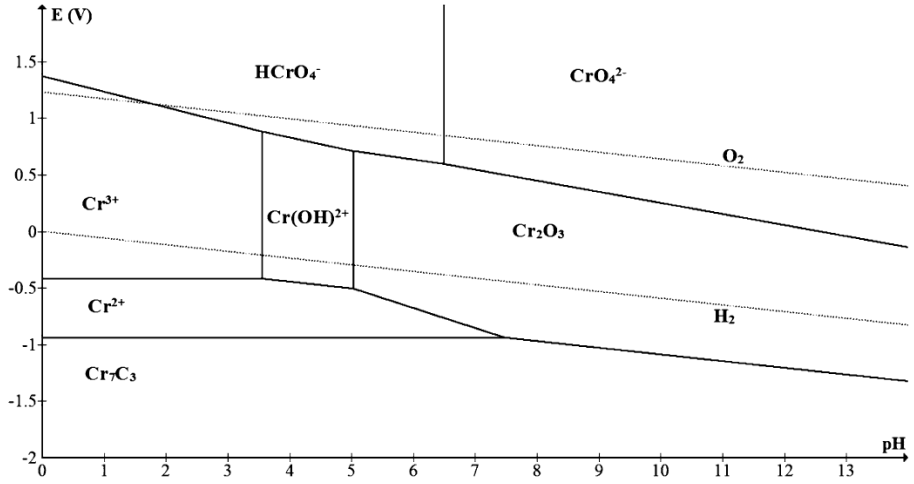

Figure 5.1. Pourbaix diagram for Cr_7C_3 at 298 K (25°C) with the concentration of 10^{-6} mol/L. [74]

For alloy constituents, we need to predict the stability of more than one metal at a time. The work of ***Baes*** at ORNL is considered the key reference for this gap [75]. Figure 5.2 was the resulting Pourbaix diagram for fuel chemistry during the MSRE project [75]. The diagram was calculated from thermodynamic data obtained from Hastelloy N container and graphite exposed to fuel salt from the MSRE project [75]. The fuel salt was LiF-BeF_2-ThF_4-UF_4. Multiple constituents of alloys can be compared simultaneously on stability diagrams—e.g., alloy constituents Cr, Fe, and Ni and solid phases that are stable at higher oxide mole fractions. This Pourbaix diagram shows that only chromium in small amounts can be oxidized from the alloy when the U^{4+}/U^{3+} ratio is in the expected range of 10 to 100. Redox control was implemented with U^{4+}/U^{3+} for MSRE. The control agent and control method for mitigating corrosion for FHRs is yet to be determined; perhaps $Ce^{2+/}Ce^{3+}$ or Eu^{3+}/Eu^{2+} buffering agent could be a feasible redox control agent for FHRs [76].

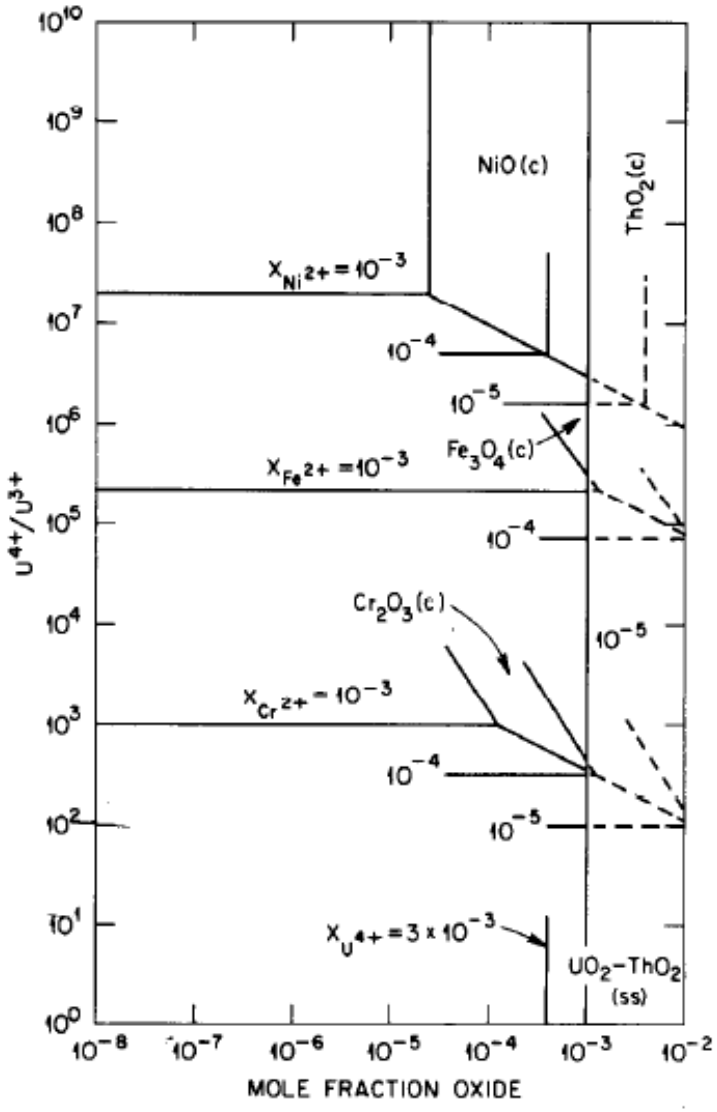

Figure 5.2. Pourbaix diagram for the structural metals in LiF-BeF_2-ThF_4 (72-16-12 mol %) at 600°C. [75]

5.1.2 SiC interactions with moisture-based impurities, tritium, and gaseous fission products

Previous sections summarized the recent work and highlight the gaps for non-irradiation experiments involving SiC and FHR materials in FLiBe and FLiNaK. Oxygen is not expected to be present in large amounts in the FHR system during normal operation. Trace moisture and air may enter the salt melt from the cover gas and from leaks. Any gaseous reactions or gaseous products, such as tritium, in the salt should be given priority. A Generation IV reactor system like the FHR should demonstrate inherent safety but also have a minimal environmental impact. Gases always risk environmental release.

The post-Fukushima tritium release was an important lesson learned and caused a loss of public confidence and trust. For some MSRs, tritium capture, control, and mitigation analyses are necessary if the tritium is not burned in-situ. It is desirable to demonstrate tritium capture and control on the level of current LWRs (2.2 Ci/GW_e·day or 810 Ci/GW_e·year). The following section current work with tritium interactions,

release, capture, and control are discussed along with SiC and tritium interactions to identify the key research gaps.

The extensive research on fission product transport/retention in TRISO fuels for other reactor systems like advanced gas-cooled reactors or even LFMSRs. It is important to recognize that for SiC materials in FHRs intended for use in non-fuel assemblies and components, lack of knowledge regarding the effects of fission product impurities in the salt reacting with SiC is also a significant gap.

5.1.2.1 SiC and intrinsic oxidants

Highly crystalline composites are desired because they have a stronger chemical bond between the Si and C. ***Yang et al.*** showed that SiC variants with higher oxygen impurities are more corroded by FLiNaK than are purified SiC variants. The purest SiC was corroded slightly by oxygen impurities in the FLiNaK. Single-crystal SiC and very high-purity CVD SiC (0.999995 %) were only slightly corroded in FLiNaK at 700°C for 10 and 45 days [77]. XPS elemental surface technique was used to detect oxygen and Si^{3+} oxidation states on the corroded samples. Silicon was detected in the salt with Inductively Coupled Plasma Optical Emission Spectrometry (ICP-OES). Oxygen contamination of FLiNaK probably aggravated the slight corrosion of SiC. The oxidation of SiC is expected to increase with temperature but currently there is a lack of experimental validation.

One potential fabrication constraint is the impurity content/purification of SiC, because oxygen contamination during composite densification processes have shown to drive preferential oxidation in molten fluoride salt. The normal levels of impurities circulating in the molten salt and the gases above the salt are not well known. Another potential gap is the effect of SiC oxidation/SiC purity on the redox control.

Wang et al. showed that the corrosion of SiC composites accelerated with temperature but the interlayer boundary in the SiC matrix was preferentially corroded because of higher intrinsic oxygen content [78]. The Si-O bond in the O-containing SiC phase was attacked by free F- anions at 800 to 1000°C for 500 hours in the salt to form Si-F bonds (SiF_6 decomposing to SiF_4 that escapes the melt). The results tend to show that oxygen in SiC accelerates the corrosion of SiC in fluoride salts. Corrosion would result from the loss of silicon in SiC, with graphite as a reaction product [80]. EDS scans showed that oxygen content in interlayer boundaries is slightly higher than in the matrix, probably because of the repetitive densification process. The interlayer boundaries and then the matrix around the residual pores in fiber-reinforced SiC_f/SiC were corroded, and the corrosion was non-uniform. Micrographs showed exfoliation of the composite surface. Gaps in the matrix probably resulted from selective corrosion of interlayer boundaries, and the gaps in the matrix then increased the porosity in the composites. Wang et al. studied a CVI SiC composite material. Unlike the corrosion in CVD SiC, non-uniform corrosion of CVI SiC_f/SiC composites in molten fluoride salt was observed.

A study at the University of Wisconsin–Madison showed that CVI-SiC lost more weight than CVD-SiC when both were exposed to FLiBe at 700°C for 1000 hours continuously. Figure 5.3 shows the results of these corrosion tests on several materials. These are preliminary studies and unpublished work.

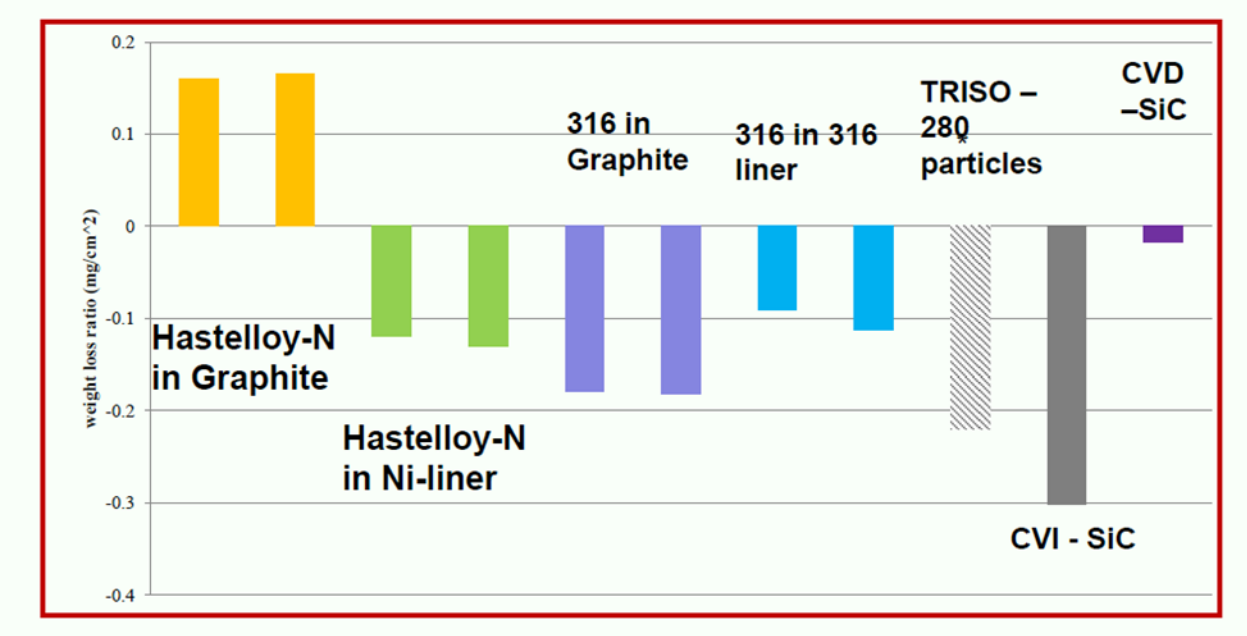

Figure 5.3. Results of University of Wisconsin–Madison testing at 700°C for 1000 hours of various materials in FLiBe for FHR. Vertical axis indicates mass loss with a net loss being negative. All test specimens were placed in a graphite container except CVI-SiC and CVD SiC were placed in a graphite container [79].

The capsule material for the SiC samples were not specified in the above study.

5.1.2.2 Tritium interaction with SiC

Tritium control and capture is a major challenge for MSRs. In a recent study, the tritium production rates were predicted for FHRs (Table 5.1).

Table 5.1. Tritium production rates by reactor compared with calculated values for FHRs using TRIDENT. [80].

	Tritium production rates		
	(Bq/GWd)	(Ci/GWd)	(g/GWd)
BWR[a]	4.6E+11	12.3	1.27E−3
PWR[a]	5.1E+11	13.9	1.43E−3
HTGR[a]	6.8E+11	18.5	1.91E−3
Fast Reactor[a]	9.2E+11	24.9	2.57E−3
Heavy Water Reactor [a]	4.4E+13	1176	0.12
FHR	BOL: 3.7E+14 EQ: 1.1E+14	BOL: 10129 EQ: 2931	BOL: 1.04 EQ: 0.30

The main pathways for in-core tritium production are shown in the nuclear reactions in Eqs. (2) – (4) [80], and the decay of ^{6}He is shown in Eq. (5).

$$ {}^{6}_{3}LiF + {}^{1}_{0}n \rightarrow {}^{3}_{1}HF + {}^{4}_{2}\alpha \, . \quad (2) $$

$$ {}^{7}_{3}LiF + {}^{1}_{0}n \rightarrow {}^{3}_{1}HF + {}^{4}_{2}\alpha + {}^{1}_{0}n' \, . \quad (3) $$

$$^{9}_{4}BeF_2 + ^{1}_{0}n \rightarrow ^{4}_{2}\alpha + ^{6}_{2}He + 2F\ . \quad (4)$$

$$^{6}_{2}He \rightarrow ^{6}_{3}Li + e^{+} + \gamma_e \text{ (t ½ = 0.8 s).} \quad (5)$$

TF corrodes metals by the reaction shown in Eq. (6). There is a constant source of tritium generation because of ^{6}Li activation and to a lesser extent ^{9}Be activation. Fluorine does not activate easily; it requires a fast incident neutron of about 9 MeV.

$$2TF + Cr \rightarrow CrF_2 + T_2\ . \quad (6)$$

Hydrogen and its isotopes are expected to be highly mobile in SiC, heat exchanger metals, and carbon. Hydrogen will likely exist as tritium in FHRs. Corrosion in FHRs is directly related to the production of tritium, which easily forms TF, which oxidizes metals. Relative to other alloying elements, chromium fluorides are unstable and dissolve into fluoride molten salt where chromium ions may come in electrical contact with SiC [75]. SiC has been shown to have low tritium permeability and solubility at high temperatures [81, 82]. However, SiC could be corroded when TF corrodes structural alloys.

Oya et al. studied the trapping and detrapping behavior of hydrogen isotopes in SiC and showed C-rich regions were disordered and can migrate near the salt/SiC interface as the process continues. Most of the trapping of deuterium was by C in SiC, according to Oya et al., who used thermal desorption spectrometry (TDS) and XPS [83]. Carbon had a higher mobility in SiC and was "freer" to interact with deuterium. The lower binding energies in the high-resolution XPS scan of the SiC Si_{2p} peak corresponded to silicon and defect interactions rather than silicon and deuterium interactions. Oya et al. also looked at deuterium interaction with damanged SiC structures. He^{+} ion implantation was followed by deuterium implantation. Even for the damaged structures, it was reasonably concluded that the retention of deuterium bound to silicon was largely decreased compared with the deuterium bound to C. This indicated that damage mainly affects the deuterium trapping site with Si (the carbon vacancies). Thus, displacement of C atoms would occur [84].

Nishimura et al. showed that tritium release (H_2 activity and F^{-} activity) and corrosion behavior depended on the redox potential in the system in an in situ tritium release experiment. TF evolves to HT (elemental tritium) and to T_2 with increasing P_{H2}. Redox agents can be used to control the relative amounts of TF and T_2. While TF cannot escape the system, T_2 and molecular T can difuse through hot metals and heat exchanging units. If proper redox control is used to prefer the formation of T_2 over TF, then the next steps are proving methods for in-core and out-of-core capture of tritium so that it does not exceed legal release limits or methods for slowing the escape of T_2 from the system [85]. One such method for controlling the tritium transport rate is via isotopic exchange, wherein hydrogen is introduced into the cover gas to convert TF to TH; but this method must be proved, along with viable redox control methods.. Molecular tritium has the lowest solubility among the released tritium forms in FLiBe and tends to permeate through structural walls more readily than other released tritium species. The tritium generated by T_2 has a large diffusivity in structural materials. Redox control is key to selecting and developing tritium recovery systems and confinement systems in the FLiBe blanket system for the Force-Free Helical Reactor (FFHR); and should be no different from the analysis required to evalute tritium corrosion and capture in FHRs. Nishimura et al. recommended developing protective coatings based on thermochemical equilibria calculations [85, 86,].

Stempien et al. have developed a model for testing different methods to limit tritium release or capture tritium based on its generation, corrosion, and transport [81]. For instance, TRIDENT has been used to model an FHR with a carbon bed for tritium update and removal. Although the model has been validated for only a limited range of available data currently, the results are very promising. The challenges with tritium include removal of tritium from the salt and developing the required capture systems to satisfy the

legally allowable tritium release limits. The trade-off is between high-efficiency removal of tritium from the salt and effective barriers to slow tritium transport through metals. Workshops have been held to coordinate research efforts, and a summary of the workshop results is available from ***Forseberg et al.*** [87, 88]. ***Calderoni et al.*** have assessed tritium permeation in the salt [89].

Tritium will likely exist as some ratio of T_2 /TF in the FHR system. TF can corrode container alloys and continually introduce metal impurities into the salt that attack SiC. Molecular T_2 can dissociate and atomic tritium can permeate SiC and become trapped in vacancy defects of irradiated SiC. The trapping behavior of tritium in structural SiC is very undesirable because it affects tritium capture and mitigation in the FHR system, and it is not well known how tritium interactions with radiation defects can affect the microstructural properties of SiC that we value.

5.2 THERMOPHYSICAL PROPERTIES OF SALTS

Knowledge of salt chemistry is key to understanding the corrosion environment. The salt is the most dynamic component of the system. The molecular dynamics, chemical inventory, and flocculation/dispersion behavior (the ability of particles, atoms and molecules in the salt to interact with one another) of just the FLiBe itself are of great interest.

There is a considerable knowledge basis for the thermophysical properties of salts that have been optimized for use with nuclear fuels and nuclear materials. Although FLiBe and FLiNaK are two strongly preferred basic fluoride salts for FHRs, other coolant salts have been examined in light of the drawbacks of Hastelloy N corrosion in FLiBe discovered during the MSRE in the 1960s [90]. FLiBe is a preferred salt with good neutronic and thermal-hydraulic. For coolant salts, an important consideration is the salt melting point. The salts are used in mixtures to reduce melting points and importantly. The salts are used in mixtures to reduce melting points and, importantly, lithium lowers melting points and also improves the heat transfer characteristics of the mixture. The main disadvantage to the ^{6}Li in the salt is tritium production, as shown in Equation (1)-(4).

Besides the fluoride salts, chloride salts are also suggested for fast breeder LFMSRs but not for thermal spectrum FHRs. They have a higher thermal neutron absorption cross-section than fluoride salts, but they also generate unfavorable Cl^{36} isotope (ßmax = 0.71 MeV) [91]. Magnesium chloride salts have been considered for the intermediate salt loop and for the DRACS secondary loop for a PB-FHR [92]. Savannah River researchers looked at $MgCl_2$-KCl to study and monitor salt potential with magnesium when it interacts with Haynes 230. They showed some preliminary results that suggest magnesium inhibits corrosion when added, evinced by a lower redox potential.

The choice of salt for FHRs involves many aspects, but the base case considers the two salts that have the better thermal and neutronic properties, not necessarily the best chemical properties. The following section includes a survey of several candidate salts other than FLiBe and FLiNaK; their benefits are discussed and their chemical compatibility with SiC is considered. Each candidate salt has a set of benefits and detriments.

The tritium and fission products transport in FLiBe for FHRs is a significant knowledge gap. The tritium transport behavior in the salt must be studied with SiC corrosion.

5.2.1 Physical Chemistry of Candidate Coolant Salts

The proposed coolant salts are mixtures with different salt components mixed to form either a binary (X-Y) or tertiary (X-Y-Z) multi-component system. The mixtures are denoted with molar percentages of each component and have a lower melting point than each individual component salt. For FHRs, the primary

candidate salts are fluorides because of their low melting points, chemical stability for high-temperature applications (> 800 °C), good compatibility with graphite, and favorable neutronic properties.

In the FHR system, there is a primary coolant loop and an intermediate/secondary heat transfer loop. For FHRs, the proposed base case primary coolant salt is *67LiF-33BeF$_2$ (FLiBe)* and the candidates for intermediate and DRACS salts are *46.5LiF-11.5NaF-42KF* (FLiNaK) or *58KF-42ZrF$_4$* or even FLiBe; the stoichiometry is represented in mole percent. FLiBe, in particular, is a basic binary salt mixture used in the MSRE in the 1960s at ORNL with some success. FLiNaK is a strongly basic tertiary salt that has similar thermophysical properties to FLiBe. Most of the current out-of-core experiments use FLiNaK as a surrogate for FLiBe in thermal/fluid experiments to avoid toxicity/safety issues with beryllium handling [93]. Table 5.2 shows a summary of measurements and estimations of some of the major thermophysical properties of interest (melting point, boiling point, density, heat capacity, volumetric heat capacity, thermal conductivity, and viscosity at the conditions noted) for the candidate coolant salts and other coolants for comparison [91, 95-99]. The salt *8NaF-92NaBF$_4$* is shown as a reference for the historical candidate coolant salt for the Molten Salt Breeder Reactor at ORNL in the 1970s. For the values referenced in Table 5.2, only a single set of conditions (temperature and pressure) are shown. Adequate experimental validation is still needed to confirm the validity of empirical models based on temperature for the density, heat capacity, thermal conductivity, viscosity, and vapor pressure of candidate coolant salts.

Table 5.2. Coolants and their thermophysical properties, measured and extrapolated from various sources.

Coolant	T_{mp} [°C]	T_{boil} [°C]	P [kg/m3]	C_p [kJ/kg °C]	ρC_p [kJ/m^3 °C]	K [W/m °C]	ν^*10^6 [m^2/s]
FLiBe (Li_2BeF_4) 700°C, 1 atm	459	1430	1940	2.42	4670	1	2.9
FLiNaK (700°C, 1 atm)	454	1570	2019	0.45	909	0.9	
58%KF-42%ZrF_4 (700°C, 1 atm)	390	1450	2795	0.251	702	0.39	
8%NaF-92%$NaBF_4$ (700°C, >1 atm)	385	700	1750	1.51	2640	0.5	0.5
Sodium (550°C)	97.8	883	820	1.27	1040	62	0.12
Lead	328	1750	10540	0.16	1700	16	0.13
Helium (7.5 Mpa)	–	–	4	5.2	20	0.29	11
Water (290°C, 7.5 Mpa)	0	290	732	5.5	4040	0.56	0.13

Generally, bases (basic salts) donate F- ions, and acids (acid salts) react with free F- ions to form complexes. Complex formation decreases activity coefficients. Forsberg et al. state the difference in the Gibbs free energy for container alloys was >20 kcal/mol·°C, but this difference in free energy is not known for SiC or for the candidate salt [87, 88]. This issue is related to the previous discussion regarding corrosion potentials.

5.2.1.1 FLiBe — (basic) primary coolant/ PRACS

FLiBe was extensively studied by ORNL in the 1960s for development of the MSRE and the Molten Salt Breeder Reactor, in which the in-core material was graphite and out-of-core structures were made of nickel-based Hastelloy N. The binary phase diagram for eutectic FLiBe is shown in Figure 5.4 [100], which shows two eutectic points, but only the chemical composition on the LiF-rich side (~0.33 mole fraction of BeF_2, T_{max} = 495.1) is favored for reactor coolants. There is considerable agreement regarding the basic shapes of the phase diagrams for FLiBe, but there are variations from study to study because the contamination level of oxygen in “pure” or “purified” FLiBe is unknown.

A feasible salt purification method is a potential technical gap for FHRs.

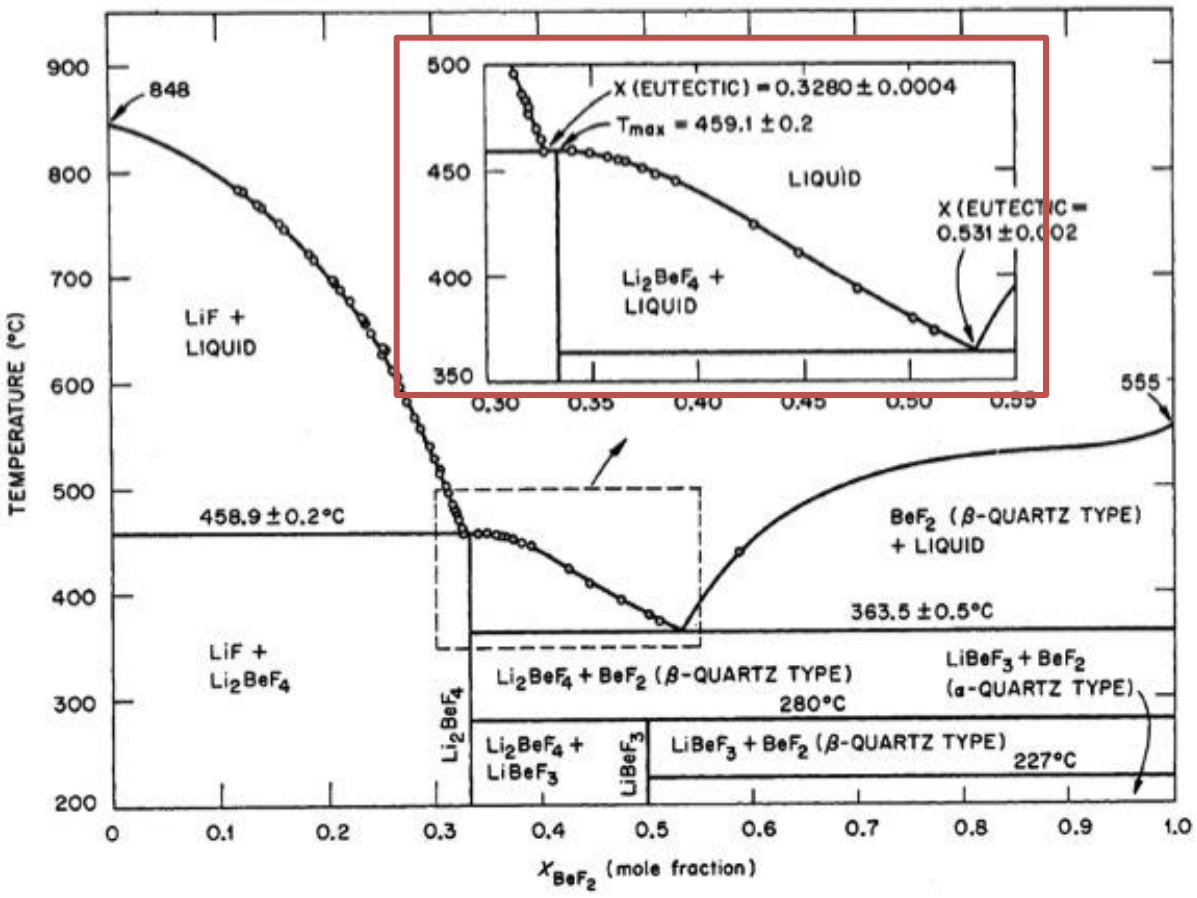

Figure 5.4. Phase diagram for FLiBe, eutectic composition and temperature highlighted in orange. [100].

5.2.1.2 FLiNaK — (strongly basic), intermediate and DRACS

In this section, the physical properties of molten salts are discussed to describe the chemical environment the SiC composites will be exposed to.

Recent chemical analysis of FLiNaK via GD-MS for is shown in Table 5.3 [100]. The salt was prepared and purified by Shanghai Institute of Organic Chemistry.

Table 5.3. Concentration of impurities in FLiNaK salt (ppm). [100]

Be	B	Mg	Al	Si	P	S	Cl	Ca	Ti	V	Cr	Mn	Fe	Co	Ni	Cu	Zn	Zr	Mo	Pd	Ag	I	Cs
<0.1	0.25	2.3	17	45	3.7	5.2	4.3	66	<0.5	0.12	20	4.2	47	<0.5	15	<1	<2	<0.5	<20	<0.5	<0.5	1.4	<0.5

For the FLiNaK tertiary phase diagram, one eutectic invariant point (T=726 K [453°C], 46.5-11.5-42.0 mol % eutectic composition) was experimentally determined by Bergman and Dergunov [101] and reconfirmed by Benes et al. in 2009 using differential scanning calorimetry [100]. Figure 5.5 shows the calculated liquid surface phase diagram of FLiNaK with one ternary eutectic point and several binary eutectics on boundary curves [100]. A correlation predicting the heat transfer of FLiNaK is desired for the design of heat transfer equipment. Some sources of uncertainty for the heat transfer predictions are due to the high operating

temperature of the reactor (700°C), optical transparency of the salt to infrared, and radiative heat transfer effects between hot and cold surfaces. The Dittus-Boelter heat transfer correlation has been shown to reasonably predict FLiNaK for turbulent conditions, but radiative heat transfer might become significant for high temperature and laminar flow [100].

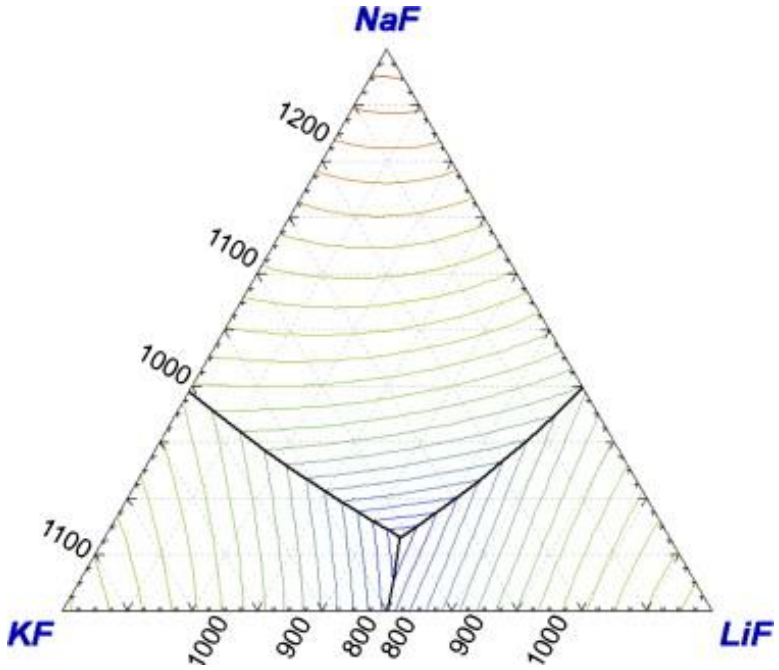

Figure 5.5. Calculated liquid surface of the FLiNaK phase diagram showing ternary eutectic point and isotherms in 25 K intervals. [100].

5.2.1.3 58%KF-42%ZrF4 (strongly acidic) candidate salt for intermediate coolant/DRACS

$KF\text{-}ZrF_4$ phase diagrams were calculated and are compared with experimental differential thermal analysis curves in Figure 5.6 [102]. The eutectic temperature of this salt mixture is lower, 390°C (663 K), and the eutectic composition contains 42 mol % ZrF_4. Nitrates, sulfates, and carbonates all contain oxygen and thus are not favorable for FHRs at higher temperatures because the salt will decompose to release oxygen. These compounds are not as stable as fluoride salts and are less favored.

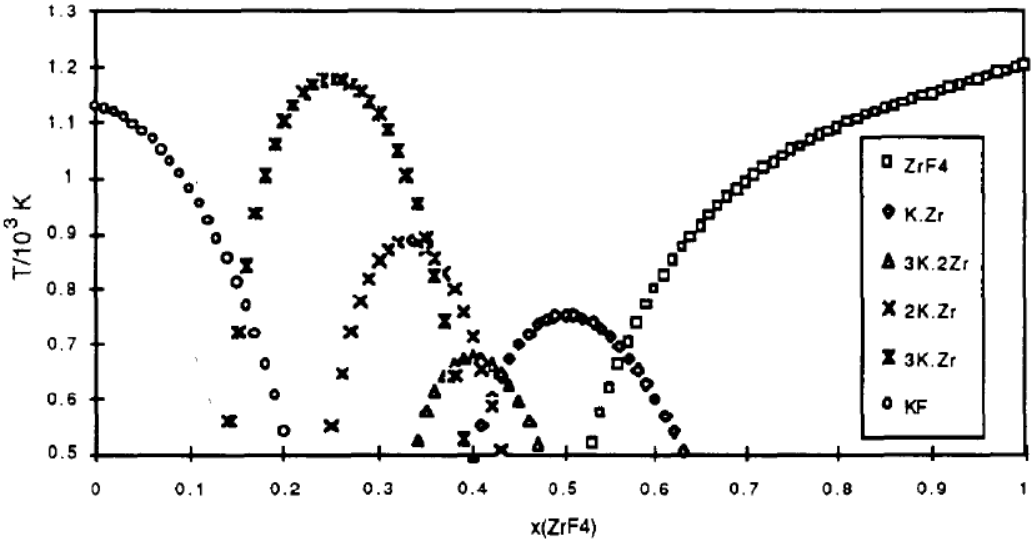

Figure 5.6. Phase diagram for KF-ZrF4 binary phase diagram. [102].

5.2.1.4 5.2.1.4. 8%NaF-92%$NaBF_4$ — fluoroborate candidate salt, heat transfer coolant

This salt is a potential candidate for the intermediate or secondary loop coolant because the tritium retention of the salt is much better than that of FLiBe. Figure 5.7 shows the phase diagram for NaF-$NaBF_4$ [100]. There is a single eutectic composition that contains 92 mol% $NaBF_4$ at a eutectic T= 658 K (385°C). Silicon carbide interactions with this salt are unknown.

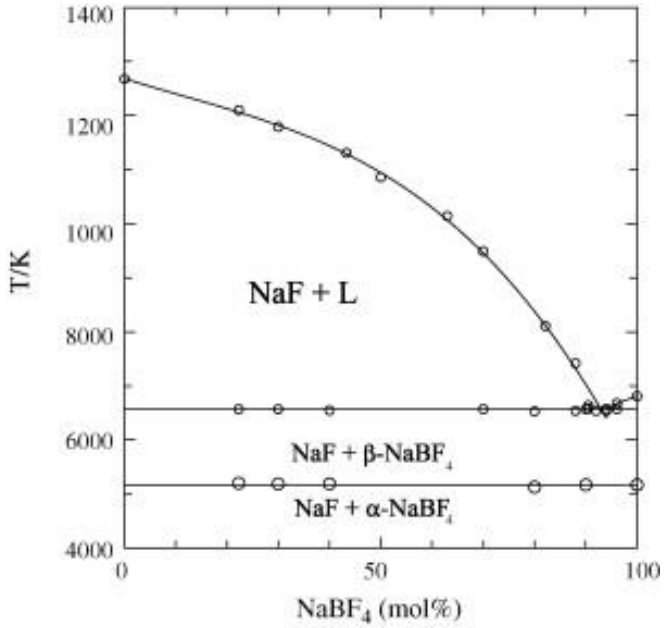

Figure 5.7. Equilibrium phase diagram of NaF-$NaBF_4$.[100].

FLiBe and FLiNaK seem to be the best options. There is considerable industry experience with other molten salts, but they have not shown the stability of FLiBe for neutronics, thermal properties, and safety margins.

5.3 THE TECHNOLOGY GAPS FOR CHEMICAL COMPATIBILITY

The corrosion of SiC in molten fluoride salts is a part of a larger corrosion issue for the container alloys. It is desirable for the SiC_f/SiC components of the core to last the lifetime of the reactor, and the time-dependent radiation stresses must be considered with the corrosion behavior.

In situ corrosion monitoring experiments are needed to prove methods of redox control. The molecular dynamics of the salt and the gradients in the system will be better demonstrated by thermal and forced convection loops. It is reasonable to imagine low-pressure systems with laminar flow velocity profiles, but a range of conditions is desired. Well-controlled experiments and robust models will be needed to describe the corrosion behavior of SiC in diverse chemical environments and to predict the longevity of irradiated SiC components. The effects of microstructure, although not the subject of this survey, will also become important because of their effect on the reactivity of the SiC matrix in fiber-reinforced SiC_f/SiC composites and the time-dependent radiation stresses induced on SiC [103].

Most of the corrosion control technologies focus on controlling the electrolyte (salt) chemistry. The properties of SiC could potentially be customized to improve its corrosion resistance in FHR. For instance, the development of SiC composites and variants with higher electrical resistivity may improve performance. Better fabrication methods will reduce gradients and performance defects.

Corrosion studies of metals should be extended to SiC. The forced convection tests could effectively simulate flow conditions, and the natural convection tests effectively simulate temperature gradients.

The following technical gaps have been identified for the task of determining SiC stability in molten fluoride salts in the presence of metals, graphites, tritium and other impurities:

- The thermodynamics of SiC corrosion in FLiBe and FLiNaK, including solubilities.
- Corrosion rate characterization and kinetics for SiC in FLiBe and FLiNaK in diverse chemical environments.
- Stability diagrams for predicting the possible stable (equilibrium) phases, corrosion reactions, and corrosion products of SiC, alloy constituents, and graphite interactions in FLiBe and FLiNaK, respectively.
- Fuel failure rate and analysis of SiC corrosion from fission products in FLiBe.
- Time-dependent stresses and SiC corrosion.
- SiC compatibility with chloride salts.
- Salt chemistry and molecular dynamics, in general, as they affect corrosion rates.
- The mitigation method for tritium fission products (in the case of liquid fuel designs) and other impurites must be compatible with SiC, and interactions need to be addressed.

6. CONCLUSION AND PATH FORWARD

This report highlights the technology gaps that exist for SiC_f/SiC composite materials if they are to be used in MSRs. It focuses mainly on FHR technology with some reference to LFMSRs. It addresses four areas of major concern: design methods and rules required for licensing, materials and manufacturing constraints and techniques, properties and radiation effects of irradiated materials, and chemical compatibility.

The design code and rules are near completion and will be adopted within the ASME BPVC Section III Division 5 within the near future. The code needs to be supported with a technical basis document that contains benchmarking data for typical designs. Continuation of additional test standard development is suggested, more specifically for the MSR environment, followed by round robin testing once standards are developed.

The fabrication of large and complex-shape components made of nuclear-grade SiC_f/SiC composites is currently practiced and may be beneficial for some MSR applications. Although processing elements and joining/integration technologies are available, demonstration of component fabrication will be required.

Joining and integration technologies are available for fabrication of SiC-based components. Silicon carbide–based joining layers have been demonstrated to retain strength following neutron irradiation. It is suggested that further investigation be conducted by exposing the joints to salt. Dissimilar material joints are more complex and need additional development if they should prove to be desirable for MSR technology.

The physical and mechanical property evaluation found that material degradation due to high-dose neutron irradiation is a critical feasibility issue when the application temperature is relatively low and neutron dose is high. A major technology gap is a complete understanding of the irradiation effects. SiC/SiC composites resistant to high-dose irradiation will offer a competitive advantage if it is demonstrated that the core components can last substantially longer in their operating environments. More data are required to address the synergy of neutron irradiation and the environmental effects, including salt corrosion and applied stress/thermal stress.

Additionally, slow crack growth in salt corrosion environments is a critical feasibility issue that has been insufficiently explored. Statistical assessment of cracking probability, understanding of the nature of cracks under different loading and corrosion conditions, and establishment of testing procedures to investigate slow crack growth are important studies to be conducted. Comprehensive studies of the microcracking issues should provide criteria for failure of SiC_f/SiC composites due to slow crack growth in MSRs.

Silicon carbide components will be exposed to diverse chemical environments. A preferred salt for the primary coolant system is FLiBe. It is also a candidate for the intermediate loop system as is FLiNaK. Limited data exist for SiC behavior in chloride salts. Further experiments are needed to determine if SiC could be used in chloride salt MSRs.

Silicon carbide exhibits wettability and chemical reactivity with metals but is generally stable in molten fluoride salts so long as the salt purity is maintained. Thermal loop testing of SiC has not been performed; but it is believed that thermal gradients could sustain corrosion in FHRs, whereas impurities-based corrosion is limited by solubilities and concentration. At controlled concentration levels, the corrosion of SiC in molten fluoride salt depends directly on the redox condition of the salt and the various methods used to mitigate impurities and tritium.

Tritium is a concern because the corrosion behavior of SiC is directly related to tritium capture. Furthermore, hydrogen and its isotopes are highly mobile in SiC. For the safe control of the tritium produced in the reactor, its retention and diffusion through the reactor materials must be known. The solubility of tritium and lattice diffusion behavior in irradiated SiC should be studied in conjunction with surface corrosion.

Corrosion testing can consist of static experiments in sealed capsules or dynamic loop experiments (thermal or forced convection). The static tests have demonstrated their practicality but are prone to errors, and oxygen in leakage could show a much higher corrosion rate than is actually caused by the pure salt. Loop testing of SiC has not yet been performed but would be beneficial to more accurately simulate reactor conditions.

Silicon carbide–based materials have many inherent properties that make them promising candidates for use in MSRs. However, before deploying a SiC/SiC composite in a MSR, there are several issues that must be resolved, and some of them are specific to the conditions of individual reactor designs. Throughout the text, several technology gaps are identified along with initial recommendations for how to address the gaps. The next step is to develop a detailed roadmap to show the development path of SiC composites for MSR applications.

7. REFERENCES

7.1 SECTION 1

[1] H.D. Gougar et al., *Assessment of the Technical Maturity of Generation IV Concepts for Test or Demonstration Reactor Concepts*, INL/EXT 15-36427 Rev 2, Idaho National Laboratory, Idaho Falls, ID, October 2015.

[2] A. Qualls et al., Preconceptual design of a fluoride high temperature salt-cooled engineering demonstration reactor: Motivation and overview," *Annals of Nuclear Energy* 107 (2017) p.144-155.

7.2 SECTION 2

[3] C.W. Forsberg et al., "Tritium control and capture in salt-cooled fission and fusion reactors," *Fusion Science and Technology* 71(4) (2017) 584-589.

[4] C.W. Forsberg, et al., "Tritium control and capture in salt-cooled fission and fusion reactors: Status, challenges, and path forward," *Nuclear Technology* 197(2) (2017) 119-139.

[5] D.E. Holcomb et al., *Fluoride Salt-Cooled High-Temperature Reactor Technology Development and Demonstration Roadmap*, ORNL/TM-2013-401, Oak Ridge National Laboratory, September 2013.

[6] C. Andreades et al., *Technical Description of the 'Mark 1' Pebble-Bed Fluoride-Salt-Cooled High Temperature Reactor (PB-FHR) Power Plant*, UCBTH-14-002, Department of Nuclear Engineering, University of California, Berkley, CA, September 2014.

[7] Xingtai Zhou, "Current Status of TMSR and the Consideration of Its Materials," NEUP Integrated Research Project Workshop, Madison, WI, Aug. 2012.

[8] Lance K. Kim, "Molten Salt Reactor Technical Working Group Licensing Perspective," GAIN Fuel Safety Research Workshop, Idaho Falls, ID. May 2017

[9] Hongjie Xu, "Status and Perspective of TMSR in China," PSI, Switzerland, January 2017.

[10] J. Serp et al., "The molten salt reactor (MSR) in generation IV: Overview and perspectives," *Progress in Nuclear Energy* 77 (2014) p308-319.

[11] International Atomic Energy Agency, *Advances in Small Modular Reactor Technology Developments*, A supplement to IAEA Advanced Reactors Information Systems (ARIS), 2016 Edition, http://aris.iaea.org.

[12] Michael J. Eades et al., "The influence of Xe-135m on steady-state xenon worth in thermal molten salt reactors," *Progress in Nuclear Energy* 93 (2016) p397-405.

[13] Per Peterson, "Overview of FHR-Specific Primary and Intermediate Loop Environments," NEUP Integrated Research Project Workshop, Madison, WI, Aug. 2012.

[14] Transatomic, Technical White Paper, November 2016 V2.1, ww.transatomicpower.com/wp-content/uploads/2015, March 2018.

[15] *Fluoride-Salt-Cooled, High-Temperature Reactor (FHR) Development Roadmap and Test Reactor Performance Requirements White Paper*, UCBTH-12-004, Massachusetts Institute of Technology, June 2013..

[16] Transatomic Power, Technical White Paper, March 2014 V1.01,www.large.stanford.edu/courses/2015/ph241/khalaf1/docs/TAP_White_Paper.pdf, accessed May 2018.

[17] D. Koch, "Microstructural Modeling and Thermomechanical Properties," *Ceramic Matrix Composites—Fiber Reinforced Ceramics and Their Application*, Ed. W. Krenkel, Wiley-Koch, 2008, p. 231-259

[18] S.R. Greene et al., *Pre-Conceptual Design of a Fluoride-Salt-Cooled Small Modular Advanced High-Temperature Reactor (Sm-AHTR)*, ORNL-TM-2010/199, Oak Ridge National Laboratory, December 2010.

[19] A. Qualls et al., *Fluoride Salt-Cooled High Temperature Demonstration Reactor Point Design*, ORNL/TM-2016/85, Oak Ridge National Laboratory, Oak Ridge, TN, February 2016.

[20] D.E. Holcomb, D. Ilas, V.K. Varma, A.T. Cisneros, R.P. Kelly, J.C. Gehin, *Core and Refueling Design Studies for the Advanced High Temperature Reactor*, ORNL/TM-2011/365, September 2011.

[21] Yao Xiao, Lin-Wen Hu, Charles Forsberg, Suizheng Qiu, Guanghui Su, Kun Chen, Naxiu Wang, "Analysis of the limiting safety system settings of a fluoride salt–cooled high-temperature test reactor," *Nuclear Technology*, 187:3, 221-234, 2014. DOI: 10.13182/ NT13-93

[22] V. Varma. et al., *AHTR Mechanical, Structural and Neutronic Preconceptual Design*, ORNL/TM-2012/320, Oak Ridge National Laboratory, Oak Ridge, TN, September 2012.

[23] N.R. Brown et al., "Preconceptual design of a fluoride high temperature salt-cooled engineering demonstration reactor: Core design and safety analysis," *Annals of Nuclear Energy* 103 (2017) p.49-59.

[24] N. Le Brun et al., "Tackling Coolant Freezing in Generation-IV Molten Salt Reactors," Proceedings of the 2017 25th International Conference on Nuclear Engineering, ICONE25, Shanghai, China, Jul 2-6 2017.

[25] ASTM C1793-15, *Standard Guide for Development of Specifications for Fiber Reinforced Silicon Carbide-Silicon Carbide Composite Structures for Nuclear Applications,* ASTM International, West Conshohocken, PA, 2015, www.astm.org

[26] Per Peterson, Todd Allen, "FHR Structural Mechanics Part 1: Characteristic Design Basis Events, Figures of Merit and Key Phenomena," NEUP Integrated Research Project Workshop, Berkley, CA, Feb 2012.

[27] R. O. Scarlat et al. "Design and licensing strategies for fluoride-salt-cooled high-temperature reactor (FHR) technology," *Progress in Nuclear Energy* 77 (2014) p.406-420.

[28] Raluca Scarlat, Mike Laufer, "FHR System Decomposition and Regulatory Design Criteria," NEUP Integrated Research Project Workshop, Berkley, CA, Feb 2012.

[29] Raluca Scarlat, Tommy Cisneros, "FHR Functional Requirements for Key Systems and Sub-Systems – Nuclear Heat Supply and Main Support Systems Areas," NEUP Integrated Research Project Workshop, Berkley, CA, Feb 2012.

[30] *Draft report on the NRC Vision and Strategy: Safely Achieving Effective and Efficient Non-Light Water Reactor Mission Readiness*, US Nuclear Regulatory Commission, ML16139A812.

[31] *Licensing Technical Requirements Modernization Project*, US Nuclear Regulatory Commission, ML17013A140.

7.3 SECTION 3

[32] Y. Katoh, K. Ozawa, C. Shih, T. Nozawa, R.J. Shinavski, A. Hasegawa, L.L. Snead, "Continuous SiC fiber, CVI SiC matrix composites for nuclear applications: Properties and irradiation effects," *J. Nucl. Mater*. 448 (2014) 448–476. doi:10.1016/j.jnucmat.2013.06.040.

[33] W.A. Curtin, “Theory of mechanical properties of ceramic-matrix composites,” *J. Am. Ceram. Soc*. 74 (1991) 2837–2845. doi:10.1111/j.1151-2916.1991.tb06852.x.

[34] J.A. DiCarlo, H.-M. Yun, “Non-oxide (silicon carbide) fibers,” *Handb. Ceram. Compos*., Springer US, 2005: pp. 33–52. doi:10.1007/0-387-23986-3_2.

[35] C. Sauder, “Ceramic matrix composites: Nuclear applications,” *Ceram. Matrix Compos*. *Mater. Model. Technol*., 2014: pp. 609–646. doi:10.1002/9781118832998.ch22.

[36] B. Budiansky, J.W. Hutchinson, A.G. Evans, “Matrix fracture in fiber-reinforced ceramics,” *J. Mech. Phys. Solids*. 34 (1986) 167–189. doi:10.1016/0022-5096(86)90035-9.

[37] J. Lamon, “Chemical vapor infiltrated SiC/SiC composites (CVI SiC/SiC),” *Handb. Ceram. Compos*., Springer US, n.d.: pp. 55–76. doi:10.1007/0-387-23986-3_3.

[38] Y. Katoh, S.M. Dong, A. Kohyama, “Thermo-mechanical properties and microstructure of silicon carbide composites fabricated by nano-infiltrated transient eutectoid process,” *Fusion Eng. Des*., 2002: pp. 723–731. doi:10.1016/S0920-3796(02)00180-1.

[39] C.P. Deck, H.E. Khalifa, B. Sammuli, T. Hilsabeck, C.A. Back, “Fabrication of SiC-SiC composites for fuel cladding in advanced reactor designs,” *Prog. Nucl. Energy*, 2012: pp. 38–45. doi:10.1016/j.pnucene.2011.10.002.

[40] Y. Katoh, T. Nozawa, L.L. Snead, “Mechanical properties of thin pyrolitic carbon interphase SiC-matrix composites reinforced with near-stoichiometric SiC fibers,” *J. Am. Ceram. Soc*. 88 (2005) 3088–3095. doi:10.1111/j.1551-2916.2005.00546.x.

[41] J.J. Sha, T. Nozawa, J.S. Park, Y. Katoh, A. Kohyama, “Effect of heat treatment on the tensile strength and creep resistance of advanced SiC fibers,” *J. Nucl. Mater*., 2004: pp. 592–596. doi:10.1016/j.jnucmat.2004.04.123.

[42] D. DeLeeuw, “Effects of joining pressure and deformation on the strength and microstructure of diffusion-bonded silicon carbide,” *J. Am. Ceram. Soc*. 75 (1992) 725–727. doi:10.1111/j.1151-2916.1992.tb07868.x.

[43] B. V. Cockeram, “Flexural strength and shear strength of silicon carbide to silicon carbide joints fabricated by a molybdenum diffusion bonding technique,” *J. Am. Ceram. Soc*. 88 (2005) 1892–1899. doi:10.1111/j.1551-2916.2005.00381.x.

[44] S.J. Son, K.H. Park, Y. Katoh, A. Kohyama, “Interfacial reactions and mechanical properties of W-SiC in-situ joints for plasma facing components,” *J. Nucl. Mater*., 2004: pp. 1549–1552. doi:10.1016/j.jnucmat.2004.04.285.

[45] M. Ferraris, A. Ventrella, M. Salvo, Y. Katoh, D. Gross, “Torsional shear strength tests for glass-ceramic joined silicon carbide,” *Int. J. Appl. Ceram. Technol*. 12 (2015) 693–699. doi:10.1111/ijac.12248.

[46] J.R. McDermid, R.A.L. Drew, “Thermodynamic brazing alloy design for joining silicon carbide,” *J. Am. Ceram. Soc*. 74 (1991) 1855–1860. doi:10.1111/j.1151-2916.1991.tb07799.x.

[47] Y. Katoh, L.L. Snead, T. Cheng, C. Shih, W.D. Lewis, T. Koyanagi, T. Hinoki, C.H. Henager, M. Ferraris, “Radiation-tolerant joining technologies for silicon carbide ceramics and composites,” *J. Nucl. Mater*. 448 (2014) 497–511. doi:10.1016/j.jnucmat.2013.10.002.

[48] H.E. Khalifa, T. Koyanagi, G.M. Jacobsen, C.P. Deck, C.A. Back, “Radiation stable, hybrid, chemical vapor infiltration/preceramic polymer joining of silicon carbide components,” *J. Nucl. Mater*. 487 (2017). doi:10.1016/j.jnucmat.2017.02.012.

[49] K. Suganuma, “Recent advances in joining technology of ceramics to metals,” *ISIJ Int.* 30 (1990) 1046–1058. doi:10.2355/isijinternational.30.1046.

[50] T. Nozawa, T. Hinoki, A. Hasegawa, A. Kohyama, Y. Katoh, L.L. Snead, C.H. Henager, J.B.J. Hegeman, “Recent advances and issues in development of silicon carbide composites for fusion applications,” *J. Nucl. Mater*. 386–388 (2009) 622–627. doi:10.1016/j.jnucmat.2008.12.305.

[51] L.L. Snead, T. Nozawa, M. Ferraris, Y. Katoh, R. Shinavski, M. Sawan, "Silicon carbide composites as fusion power reactor structural materials," *J. Nucl. Mater*., 2011: pp. 330–339. doi:10.1016/j.jnucmat.2011.03.005.
[52] M. Ferraris, A. Ventrella, M. Salvo, M. Avalle, F. Pavia, E. Martin, "Comparison of shear strength tests on AV119 epoxy-joined carbon/carbon composites," *Compos. Part B Eng*. 41 (2010) 182–191. doi:10.1016/J.COMPOSITESB.2009.10.008.
[53] T. Koyanagi, Y. Katoh, J.O. Kiggans, T. Hinoki, H.E. Khalifa, C.P. Deck, C.A. Back, "Irradiation resistance of silicon carbide joint at light water reactor–relevant temperature," *J. Nucl. Mater*. 488 (2017). doi:10.1016/j.jnucmat.2017.03.017.
[54] C.P. Deck, G.M. Jacobsen, J. Sheeder, O. Gutierrez, J. Zhang, J. Stone, H.E. Khalifa, C.A. Back, "Characterization of SiC-SiC composites for accident tolerant fuel cladding," *J. Nucl. Mater.* 466 (2015) 1–15. doi:10.1016/j.jnucmat.2015.08.020.
[55] K. Yueh, K.A. Terrani, "Silicon carbide composite for light water reactor fuel assembly applications," *J. Nucl. Mater*. 448 (2014) 380–388. doi:10.1016/j.jnucmat.2013.12.004.
[56] Y. Katoh, A. Kohyama, T. Nozawa, M. Sato, "SiC/SiC composites through transient eutectic-phase route for fusion applications," *J. Nucl. Mater*., 2004: pp. 587–591. doi:10.1016/j.jnucmat.2004.04.157.
[57] "Silicon Carbide (SiC) Fiber-Reinforced SiC Matrix Composites," (n.d.). https://technology.nasa.gov/patent/LEW-TOPS-25.
[58] A. Mhlratzer, H. Pfeiffer, "CMC Body Flaps for the X-38 Experimental Space Vehicle," in 26th Annual Conference on Composites, Advanced Ceramics, Materials, and Structures: A: Ceramic Engineering and Science Proceedings, Volume 23, John Wiley & Sons, Inc., n.d.: pp. 331–338. doi:10.1002/9780470294741.ch38.

7.4 SECTION 4

[32] Y. Katoh, K. Ozawa, C. Shih, T. Nozawa, R.J. Shinavski, A. Hasegawa, L.L. Snead, "Continuous SiC fiber, CVI SiC matrix composites for nuclear applications: Properties and irradiation effects," *J. Nucl. Mater*. 448 (2014) 448–476. doi:10.1016/j.jnucmat.2013.06.040.
[38] Y. Katoh, S.M. Dong, A. Kohyama, "Thermo-mechanical properties and microstructure of silicon carbide composites fabricated by nano-infiltrated transient eutectoid process," *Fusion Eng. Des.*, 2002: pp. 723–731. doi:10.1016/S0920-3796(02)00180-1.
[59] L.L. Snead, T. Nozawa, Y. Katoh, T.S. Byun, S. Kondo, D.A. Petti, "Handbook of SiC properties for fuel performance modeling," *J. Nucl. Mater*. 371 (2007) 329–377. doi:10.1016/j.jnucmat.2007.05.016.
[60] G. Newsome, L.L. Snead, T. Hinoki, Y. Katoh, D. Peters, "Evaluation of neutron irradiated silicon carbide and silicon carbide composites," *J. Nucl. Mater*. 371 (2007) 76–89. doi:10.1016/j.jnucmat.2007.05.007.
[61] Y. Katoh, T. Koyanagi, J.L. McDuffee, L.L. Snead, K. Yueh, "Dimensional stability and anisotropy of SiC and SiC-based composites in transition swelling regime," *J. Nucl. Mater*. 499 (2018). doi:10.1016/j.jnucmat.2017.12.009.
[62] T. Koyanagi, T. Nozawa, Y. Katoh, L.L. Snead, "Mechanical property degradation of high crystalline SiC fiber-reinforced SiC matrix composite neutron irradiated to ~100 displacements per atom," *J. Eur. Ceram. Soc.* (2017). doi:10.1016/j.jeurceramsoc.2017.12.026.
[63] Y. Katoh, L.L. Snead, C.M. Parish, T. Hinoki, "Observation and possible mechanism of irradiation induced creep in ceramics," *J. Nucl. Mater*. 434 (2013) 141–151. doi:10.1016/j.jnucmat.2012.11.035.

[64] T. Koyanagi, Y. Katoh, K. Ozawa, K. Shimoda, T. Hinoki, L.L. Snead, "Neutron-irradiation creep of silicon carbide materials beyond the initial transient," *J. Nucl. Mater*. 478 (2016). doi:10.1016/j.jnucmat.2016.06.006.
[65] Y. Katoh, T. Nozawa, C. Shih, K. Ozawa, T. Koyanagi, W. Porter, L.L. Snead, "High-dose neutron irradiation of Hi-Nicalon Type S silicon carbide composites. Part 2: Mechanical and physical properties," *J. Nucl. Mater*. 462 (2015). doi:10.1016/j.jnucmat.2014.12.121.
[66] K.A. Terrani, C. Ang, L.L. Snead, Y. Katoh, "Irradiation stability and thermo-mechanical properties of NITE-SiC irradiated to 10 dpa," *J. Nucl. Mater*. 499 (2018) 242–247. doi:10.1016/j.jnucmat.2017.11.040.
[67] K.A. Terrani, J.O. Kiggans, C.M. Silva, C. Shih, Y. Katoh, L.L. Snead, "Progress on matrix SiC processing and properties for fully ceramic microencapsulated fuel form," *J. Nucl. Mater*. 457 (2015) 9–17. doi:10.1016/j.jnucmat.2014.10.034.
[68] T. Nozawa, K. Ozawa, Y. Asakura, A. Kohyama, H. Tanigawa, "Evaluation of damage accumulation behavior and strength anisotropy of NITE SiC/SiC composites by acoustic emission, digital image correlation and electrical resistivity monitoring," *J. Nucl. Mater*. 455 (2014) 549–553. doi:10.1016/j.jnucmat.2014.08.043.
[69] J. Vacik, H. Naramoto, J. Cervena, V. Hnatowicz, I. Peka, D. Fink, "Absorption of molten fluoride salts in glassy carbon, pyrographite and Hastelloy B," *J. Nucl. Mater*. 289 (2001) 308–314. doi:10.1016/S0022-3115(01)00419-6.

7.5 SECTION 5

[70] W. Xue, X. Yang, J. Qiu, H. Liu, B. Zhao, H. Xia, X. Zhou, P. Huai, H. Liu, J. Wang, "Effects of Cr3+ on the corrosion of SiC in LiF–NaF–KF molten salt," *Corrosion Science* 114 (2017) 96-101.
[71] Y.P. Zaykov, A.V. Isakov, I.D. Zakiryanova, O.G. Reznitskikh, O.V. Chemezov, A.A. Redkin, "Interaction between SiO2 and a KF-KCl-K2SiF6 Melt," *J. Phys. Chem. B* 118(6) (2014) 1584-8.
[72] X. Yang, D. Zhang, M. Liu, S. Feng, W. Xue, H. Liu, G. Yu, X. Zhou, H. Xia, P. Huai, Z. Li, Y. Lu, H. Zhou, S. Dong, "Corrosion of SiC induced by Hastelloy N alloy and its corrosion products in LiF–NaF–KF molten salt," *Corrosion Science* 109 (2016) 62-67.
[73] H. Nishimura, T. Terai, T. Yoneoka, S. Tanaka, A. Sagara, O. Motojima, "Compatibility of structural candidate materials in LiF-BeF2 molten salt mixture," *J. Nuc. Mater.* 283-287 (2000) 1326-1331.
[74] V. Marimuthu, I. Dulac, K. Kannoorpatti, "Significance of Pourbaix Diagrams to Study the Corrosion Behaviour of Hardfacing Alloys Based on Chromium Carbides at 298 K (25 °C)," *J. Bio- and Tribo-Corrosion* 2(3) (2016).
[75] J. Baes, C.F., "Chemistry and Thermodynamics of Molten Salt Reactor Fuels," *J. Nuc. Mater.* 51 (1974) 149-162.
[76] S. Guo, N. Shay, Y. Wang, W. Zhou, J. Zhang, "Measurement of europium (III)/europium (II) couple in fluoride molten salt for redox control in a molten salt reactor concept," *J. Nuc. Mater.* 496 (2017) 197-206.
[77] X. Yang, M. Liu, Y. Gao, D. Zhang, S. Feng, H. Liu, G. Yu, G. Wu, M. Wang, X. Zhou, H. Xia, P. Huai, T.K. Sham, J. Wang, J. Guo, "Effect of oxygen on the corrosion of SiC in LiF–NaF–KF molten salt," *Corrosion Science* 103 (2016) 165-172.
[78] H. Wang, Q. Feng, Z. Wang, H. Zhou, Y. Kan, J. Hu, S. Dong, "Microstructure evolution and high-temperature mechanical properties of SiCf/SiC composites in liquid fluoride salt environment," *Corrosion Science* 124 (2017) 131-137.

[79] University of Wisconsin, Department of Nuclear Engineering, "Fluoride-Salt-Cooled, High-Temperature Reactor (FHR) White Paper," Integrated Research Project (IRP-2) Workshop 2, 2014.
[80] J.D. Stempien, R.G. Ballinger, C.W. Forsberg, "An integrated model of tritium transport and corrosion in Fluoride Salt-Cooled High-Temperature Reactors (FHRs) – Part I: Theory and benchmarking," *Nuc. Eng. and Des.* 310 (2016) 258-272.
[81] R. Causey, W.R. Wampler, "The use of silicon carbide as a tritium permeation barrier," *J. Nuc. Mater.* 220-222 (1995) 823-826.
[82] R. Causey, W.R. Wampler, J.R. Retelle, J.L. Kaae, "Tritium migration in vapor-deposited B-silicon carbide," *J. Nuc. Mater.* 203 (1993) 196-205.
[83] Y. Oya, Y. Onishi, T. Takeda, H. Kimura, K. Okuno, S. Tanaka, "Interaction between hydrogen isotopes and damaged structures produced by He+ implantation in SiC," *Fus. Eng. and Des.* 81(8-14) (2006) 987-992.
[84] Y. Oya, Y. Onishi, K. Okuno, S. Tanaka, "Trapping and detrapping mechanisms of deuterium in SiC studied by XPS and TDS techniques," *Mater. Trans.* 46(3) (2005) 552-556.
[85] H. Nishimura, A. Suzuki, T. Terai, M. Yamawaki, S. Tanaka, A. Sagara, O. Motojima, "Chemical behavior of Li2BeF4 molten salt as a liquid tritium breeder," *Fusion Eng. and Des.* 58-59 (2001) 667-672.
[86] T. Terai, S. Tanaka, "Tritium release behavior from liquid tritium breeding materials for fusion reactor blanket under neutron irradiation," *Progress in Nuclear Energy* 32(1) (1998) 97-112.
[87] C.W. Forsberg, D.M. Carpenter, D.G. Whyte, R. Scarlat, L. Wei, Tritium control and capture in salt-cooled fission and fusion reactors, *Fusion Science and Technology* 71(4) (2017) 584-589.
[88] C.W. Forsberg, S. Lam, D.M. Carpenter, D.G. Whyte, R. Scarlat, C. Contescu, L. Wei, J. Stempien, E. Blandford, Tritium control and capture in salt-cooled fission and fusion reactors: status, challenges, and path forward, *Nuclear Technology* 197(2) (2017) 119-139.
[89] P. Calderoni, P. Sharpe, M. Hara, Y. Oya, "Measurement of tritium permeation in FLiBe (2LiF–BeF2)," *Fusion Engineering and Design* 83(7-9) (2008) 1331-1334.
[90] J.R. Keiser, "Status of Tellurium - Hastelloy N Studies in Molten Fluoride Salts," ORNL/TM-6002, 1977.
[91] D. Samuel, "Molten salt coolants for high temperature reactors- a literature summary of key R & D activities and challenges," IAEA Intern Report, 2009.
[92] R.O. Scarlat, M.R. Laufer, E.D. Blandford, N. Zweibaum, D.L. Krumwiede, A.T. Cisneros, C. Andreades, C.W. Forsberg, E. Greenspan, L.-W. Hu, P.F. Peterson, "Design and licensing strategies for the fluoride-salt-cooled, high-temperature reactor (FHR) technology," *Progress in Nuclear Energy* 77 (2014) 406-420.
[93] D.A. Petti, G.R. Smolik, M.F. Simpson, J.P. Sharpe, R.A. Anderl, S. Fukada, Y. Hatano, M. Hara, Y. Oya, T. Terai, D.K. Sze, S. Tanaka, "JUPITER-II molten salt Flibe research: An update on tritium, mobilization and redox chemistry experiments," *Fusion Engineering and Design* 81(8-14) (2006) 1439-1449.
[94] S. Yoder, "Development of a forced convection liquid fluoride," Proceedings of HTR 2010, Prague, Czech Republic, 2010.
[95] G.L. Yoder, D. Heatherly, D. Wilson, M. Caja, "FLiNaK compatibility studies with Inconel 600 and silicon carbide," *Nuc. Eng. and Des.* 307 (2016) 172-180.
[96] J. Ambrosek, M. Anderson, K. Sridharan, T. Allen, "Current status of knowledge of the fluoride salt (FLiNaK) heat transfer, *Nuclear Technology* 165(2) (2017) 166-173.
[97] D. Wilson, L.M. Toth, K.T. Clarno, "Assessment of Candidate Molten Salt Coolants for the Advanced High-Temperature Reactor (AHTR)," ORNL/TM-2006/12, 2006.
[98] D. Wilson, Assessment of candidate molten salt coolants for the NGNP/NHI heat transfer loop, ORNL/TM-2006/69, 2006.

[99] M.D. Silverman, W.R. Huntley, H.E. Robertson, “Heat transfer measurements in a forced convection loop with two molten-fluoride salts: LiF-BeF2-ThF-UF4 and eutectic NaBF4-NaF,” ORNL/TM-5335, 1976.
[100] O. Beneš, R.J.M. Konings, “Thermodynamic properties and phase diagrams of fluoride salts for nuclear applications,” *Journal of Fluorine Chemistry* 130(1) (2009) 22-29.
[101] A.G. Bergmann, E.P. Dergunov, “Das Schmelzdiagramm des systems LiF-KF-NaF,” *Dokl. Acad. Sci. URSS* 31(753) (1941).
[102] G. Hatem, “Calculation of phase diagrams for the binary systems BaF2-KF and KF-ZrF4 and ternary systems BaF2-KF-ZrF4,” *Thermochimica Acta* 260 (1995) 17-28.
[103] J.-S. Park, H. Nishimura, D. Hayasaka, J.-H. Yu, H. Kishimoto, A. Kohyama, “Fabrication of short SiC fiber reinforced SiC matrix composites with high fiber volume fraction*,” Fusion Engineering and Design* 109-111 (2016) 1174-1178.